JBC Papers in Press. Published on June 13, 2018 as Manuscript RA118.002486
The latest version is at http://www.jbc.org/cgi/doi/10.1074/jbc.RA118.002486

Probing the correlation between insulin activity and structural stability through introduction of the rigid A6–A11 bond

Shee Chee Ong[§1], Alessia Belgi[#], Bianca van Lierop[#1], Carlie Delaine[§], Sofianos Andrikopoulos[&], Christopher A. MacRaild[π], Raymond S. Norton[π2], Naomi L. Haworth[#†‡], Andrea J. Robinson[#3] and Briony E. Forbes[§*3]

From the [§] College of Medicine & Public Health, Flinders University of South Australia, Bedford Park, 5042, Australia.
[#] School of Chemistry, Monash University, Clayton, Victoria, 3800, Australia.
[&] Department of Medicine, University of Melbourne, Parkville, Victoria, 3010, Australia.
[π] Medicinal Chemistry, Monash Institute of Pharmaceutical Sciences, Monash University, Parkville 3052, Australia.
[†] Research School of Chemistry, Australian National University, Acton, ACT 2601, Australia.
[‡] School of Life and Environmental Sciences, Deakin University, Waurn Ponds, Victoria 3216, Australia.

Running title: *A6-A11 disulfide affects insulin B chain conformation*

[*] To whom the correspondence may be addressed: College of Medicine & Public Health, Flinders University of South Australia, Bedford Park, 5042, Australia. Email: briony.forbes@flinders.edu.au; Tel: +61882044221

Keywords: Dicarba peptides, insulin, disulfide bonds, biophysical studies

The development of fast-acting and highly stable insulin analogues is challenging. Insulin undergoes structural transitions essential for binding and activation of the insulin receptor (IR), but these conformational changes can also affect insulin stability. Previously, we substituted the insulin A6–A11 cystine with a rigid, non-reducible C=C linkage ("dicarba" linkage). A *cis* alkene permitted the conformational flexibility of the A-chain *N*-terminal helix necessary for high affinity IR binding resulting in surprisingly rapid activity *in vivo*. Here, we show that, unlike the rapidly acting Lys^{B28}Pro^{B29} insulin analogue (KP insulin), *cis* dicarba insulin is not inherently monomeric. We also show that *cis* dicarba KP insulin lowers blood glucose levels even more rapidly than KP insulin, suggesting that an inability to oligomerize is not responsible for the observed rapid activity onset of *cis* dicarba analogues. While rapid-acting, neither dicarba species is stable, as assessed by fibrillation and thermodynamics assays. MALDI analyses and molecular dynamics simulations of *cis* dicarba insulin revealed a previously unidentified role of the A6–A11 linkage in insulin conformational dynamics. By controlling the conformational flexibility of the insulin B-chain helix, this linkage affects overall insulin structural stability. This effect is independent of its regulation of the A-chain *N*-terminal helix flexibility necessary for IR engagement. We conclude that high affinity IR binding, rapid *in vivo* activity, and insulin stability can be regulated by the specific conformational arrangement of the A6–A11 linkage. This detailed understanding of insulin's structural dynamics may aid in the future design of rapid-acting insulin analogues with improved stability.

Since the discovery of insulin by Banting and Best, insulin therapy remains the primary treatment for type 1 (T1D) and late stage type 2 diabetes (T2D), being prescribed to effectively lower blood glucose levels (1-3). Long-acting (eg insulin glargine; Lantus®, Sanofi) and rapid-acting insulin analogues (eg lispro insulin or KP insulin[4]); Humalog®, Eli Lilly) currently in clinical use were developed to mimic the physiological basal-bolus insulin profile (recently reviewed in Mathieu *et al.* (3)). Although these analogues are undoubtedly life-savers for diabetic patients, their pharmacokinetic and pharmacodynamic performance remains suboptimal for some patients (3). Of high priority is the development of a new rapid-acting insulin analogue possessing faster onset of action and greater structural stability. To achieve this, a deeper understanding is required of the structural determinants of insulin necessary for receptor binding and function.

Insulin is a small globular protein synthesized in the pancreatic β-cells and secreted as a two-chain polypeptide comprising a 21-residue A chain and a 30-residue B chain. The secondary structure of insulin consists of three α-helices, two within the A chain (A1 to A8 and A12 to A18, respectively) and a single α-helix within the central segment of B chain (B9 to B19) (Fig. 1, *A* and *B*) (4). It is stored in pancreatic β-cells as 2Zn-coordinated hexamers that, when released into the blood stream, rapidly dissociate into active monomers (5). The monomeric form then adopts the active conformation, and in doing so reveals essential residues within the hydrophobic core for binding (6) but also primes the molecule to the formation of higher order oligomers (7-9). This is highlighted in the rapid-acting KP insulin, an analogue possessing an inversion of Pro^{B28}Lys^{B29} in the B chain of native insulin to render the molecule essentially monomeric through disruption of the dimer interface (Fig. 1*A*) (10,11). As

a consequence, KP insulin is rapid acting, but concomitant exposure of core hydrophobic residues means that KP insulin readily forms fibrils (9,12,13). This highlights the fine balance between the competing requirements for stability and conformational plasticity needed for optimal activity.

High affinity binding to the insulin receptor (IR; a tyrosine kinase receptor (14)) is achieved by interaction through two distinct binding surfaces (1 and 2) on the ligand (6,15-17). Insulin site 1 binding residues (also known as the "classical binding site") are also involved in insulin dimerization (18,19) while site 2 binding residues overlap with the hexamer-forming surfaces within a 2Zn-insulin hexamer (Fig. 1*A*) (6,16,20). Recent crystallographic studies of an IR fragment comprised of the ectodomain and the αCT segment in complex with insulin through site 1 residues provided key insights into the mechanism of insulin:IR interaction (15,21). Key conformational changes in insulin required for effective IR binding were identified. Movement of the *C*-terminal segment (B24-B30) of the B chain from the hormone core is required for engagement with the IR αCT and L1 domains (22). It is likely that the end of the B chain opens in a zipper-like fashion (23) to allow accessibility to insulin site 1-binding residues that otherwise remain buried within the hydrophobic core (21,22). Evident in our previous findings, insulin also undergoes further conformational change within the first A chain helix to enable binding. The helix rotates in order to avoid a steric clash between the first four residue sidechains and the αCT segment (24). In this conformation, residues A1 to A5 to form a single α-helical turn while residues A3 to A9 adopt a wider helix conformation, approximating an (*i*, *i*+5) π-helix (24). This conformation is also evident in the μIR: insulin crystal structure (PDB entries 4OGA) (21,24) and can be artificially achieved by a mutation of residue B26 that also promotes opening of the B chain (25,26).

The correct folding and stabilization of the unique three-dimensional structure of mature insulin is supported by the three disulfide linkages: two inter-chain (Cys^{A7}-Cys^{B7} and Cys^{A20}-Cys^{B19}) and one intra-chain (Cys^{A6}-Cys^{A11}) (Fig. 1, *A* and *B*) (5,27). Correct disulfide combination is essential for function (27-30). The Cys^{A7}-Cys^{B7} bond is surface exposed and holds the *N*-termini of the two chains together. Both Cys^{A6}-Cys^{A11} and Cys^{A20}-Cys^{B19} linkages are buried within the hydrophobic core. Once folded, the Cys^{A20}-Cys^{B19} disulfide is constrained in a fixed configuration and buried deeply within the core, suggesting its most likely function is to maintain structural stability. The intra-chain Cys^{A6}-Cys^{A11} cystine, although buried, is relatively flexible and can adopt several different configurations (30-32). In our recent study, we identified that the Cys^{A6}-Cys^{A11} linkage is an important modulator of the structural transitions of the *N*-terminal A chain helix required for insulin activity. Introduction of two isomeric fixed A6-A11 dicarba bridges in insulin did not perturb the overall structure but resulted in strikingly different receptor potencies, where the *cis* isomer permits high affinity IR binding and the *trans* isomer does not (Figs. 1*C*, 2*A* and (24)).

Arising from our study of the *cis* dicarba insulin was the observation that this analogue promotes a more rapid lowering of blood glucose levels than native insulin. It is also less thermodynamically and chemically stable than native insulin (24). As these properties are reminiscent of the monomeric KP insulin (7,9,33), we investigate here whether the A6-A11 likage not only controls A chain flexibility but also influences the B chain conformation, leading to the monomeric state required for rapid receptor engagement.

In this study, through a combination of biophysical analyses of *cis* dicarba insulin and the monomeric *cis* dicarba KP insulin counterpart, we show that, despite its rapid action *in vivo* and its accelerated fibril formation relative to native insulin, the *cis* dicarba insulin is not inherently monomeric. Limited proteolysis studies alluded to an unexpected conformational change in the B-chain helix. Such a link between the A6-A11 disulfide and the conformational dynamics of the B chain has not been previously described. These findings suggest a key role for the A6-A11 linkage, not only in regulating A chain flexibility that primes insulin for receptor engagement, but also in influencing the B chain conformation and regulating insulin's stability.

RESULTS

Chemical synthesis of dicarba insulins – We aimed to understand the mechanism by which the *cis* dicarba insulin was apparently rapid acting *in vivo* by directly comparing its *in vitro* and *in vivo* biological and biophysical activities with the monomeric c[Δ^4A6,11]-dicarba human lispro insulin (*cis*- and *trans* dicarba KP insulins). The *cis*- and *trans*-configured dicarba insulin A chains, in which a C=C dicarba bond replaces the A6-A11 intra-chain S-S bond (Fig. 1*C*), were synthesised as previously described using a RCM and SPPS-catalysis approach (24,34). The modified dicarba insulin A chains were then combined with requisite insulin B chains to provide *cis* and *trans* isomers of c[Δ^4A6,11]-dicarba human insulin and c[Δ^4A6,11]-dicarba KP insulin. The dicarba analogues were purified by RP-HPLC (see Figs. 1, *D* and *E*, and S1) before being subjected to biological and biophysical analyses.

Cis dicarba insulin and cis dicarba KP insulin are equally potent to native insulin in receptor binding and activation – The binding affinities of the dicarba insulin analogues for the IR-B and IGF-1R were determined using competition binding assays (Figs. 2*A*, S2 and Table S1). Notably, the restrained A6-A11 *cis* and *trans* dicarba C=C bonds had the same effect when introduced into the monomeric KP insulin analogue as was previously seen with the *cis* and *trans* dicarba analogues of human insulin (24). *Cis* dicarba insulin and *cis* dicarba KP insulin were equipotent to native insulin in binding and activation of both the IR-B (Fig. 2, *A* and *B*) and the IGF-1R (Fig. S1, *A* and *B*) (Table S1), suggesting that the restrained *cis* dicarba

C=C bond allows both analogues to adopt a conformation that engages with both receptors in a manner similar to insulin. Conversely, *trans* dicarba insulin and *trans* dicarba KP insulin bind poorly to both the IR-B (Fig. 2*A*) and IGF-1R (Fig. S1*A*) (Table S1), indicating that the *trans* dicarba configuration restricts both analogues from forming a high affinity interaction with these receptors. The *trans* dicarba insulins were subsequently excluded in this and further activity assays due to their poor receptor binding affinities.

The cis dicarba KP insulin promotes in vitro DNA synthesis and glucose uptake with equal potency to native insulin – Corresponding with its IR-B binding and activation potency, the *cis* dicarba KP insulin was equipotent with native insulin in promoting DNA synthesis in L6 rat skeletal myoblast overexpressing IR-A. This is in contrast to the *cis* dicarba insulin, which was 5 to 10-fold less potent than insulin in promoting mitogenic activity (Fig. 2*C* and (24)). The *cis* dicarba KP insulin was equipotent with *cis* dicarba insulin and insulin in promoting glucose uptake in cultured NIH3T3-L1 adipocytes (Fig. 2*D*). There is a trend of lower activities for the *cis* dicarba insulin and *cis* dicarba KP insulin, however the effect was not significantly different.

The cis dicarba insulin demonstrates identical self-association behaviour to native insulin – AUC was performed in order to determine whether the *cis* dicarba insulin is monomeric as suggested by its rapid action *in vivo* (Fig. 2, *E* and *F*, and (24)). In the presence of Zn^{2+}, sedimentation equilibrium data for the *cis* dicarba insulin was fitted to a single species of apparent mass 34,500 ± 400 Da (Fig. 3*A*), consistent with the expected mass of a 2-Zn^{2+} human insulin hexamer (34,726 Da). At higher concentrations the fit was not perfect (reduced $\chi^2 \sim 4$), suggesting the presence of other high molecular weight species, consistent with previous observations for native mammalian insulins (35).

In contrast, the shape of the equilibrium concentration distributions in the absence of Zn^{2+} were clearly concentration dependent, implying reversible self-association (Fig. 3*B*). Accordingly, these data could not be fit as a single species, in sharp contrast to those we have recently described for the strictly monomeric venom insulin of *Conus geographus* (Fig. S11) (36). Native insulin shows similar concentration dependence in the shape of its equilibrium concentration distributions (Fig. S11), and also fails to fit to single-species models, consistent with its expected tendency for self-association. For an initial model-free assessment of the self-association of Zn^{2+}-free *cis* dicarba and native insulin, the data were plotted as the square of the radial position scaled by rotor speed $[\omega^2(r^2-r_0^2)]$ *vs* the logarithm of the equilibrium concentration (Fig. 3*C*). The slope of such a plot is proportional to the weight-average molecular weight of all species present at each point in the cell, and the observed non-linearity confirms the presence of multiple species in the sample. Over much of the accessible concentration range, the slopes of the *cis*-dicarba and native insulin plots are similar, implying that the self-association behaviour of the two insulins are similar. At low concentration (< 10 μM), the slope was consistent with that expected for monomeric insulin, suggesting that monomer dominated at these concentrations. The slope increased with increasing concentration, indicating that oligomeric species were dominant over much of the experimental concentration range. Only at the highest concentrations is there evidence of some divergence between the two curves, suggesting the possibility of some difference in the tendency of *cis* dicarba insulin to form higher-order oligomers.

Attempts to fit the two datasets to a specific, consistent model of self-association were unsuccessful, due to numerical instabilities in relevant models (37), and perhaps also reflecting the putative subtle difference in higher-order oligomerisation. Nonetheless, under the conditions studied, the self-association behaviour of the *cis* dicarba insulin is qualitatively similar to that of native mammalian insulins. Like native insulin, *cis* dicarba insulin is only monomeric in the absence of Zn^{2+}, and only at low concentration.

Cis dicarba KP insulin lowers blood glucose levels more effectively and more rapidly compared to the cis dicarba insulin, KP insulin and native human insulin – Having established that the *cis* dicarba insulin is not monomeric we sought to compare the *in vivo* activities of this analogue with *cis* dicarba KP insulin, which we can assume is monomeric as per KP insulin. The *cis* dicarba KP insulin lowered blood glucose levels more effectively and more rapidly compared to native insulin and KP insulin when mice were treated with 0.75 IU/kg insulin or analogue under non-fasting conditions (Fig. 2, *E* and *F*). Notably, the *cis* dicarba KP insulin was even more effective and rapid acting than the *cis* dicarba insulin. The glucose-lowering effect was most evident and significant in insulin-resistant mice fed on high fat diet (Fig. 2*F*). The difference in activities between native and *cis* dicarba KP insulin, which are both expected to be monomeric, implies that the improved activity of the *cis* dicarba analogues is not the result of a change in self-association. This is consistent with the above observation that native and *cis* dicarba insulin show similar self-association behaviour.

Cis dicarba insulin and cis dicarba KP insulin more rapidly form fibrils than native human insulin – While the rapid action of the *cis* dicarba insulin compared to insulin is not due to this analogue being monomeric, it must have different biophysical properties to insulin that lead to this difference in biological activity. To explore this further we next investigated the ability to form fibrils in an AFM fibrillation assay. The *cis* dicarba insulin formed fibrils more rapidly than native insulin, with fibrils first detected after 2 h compared to 6 h for native insulin at the same temperature and concentration (60 °C and 1.16 mg/mL, respectively, Fig. 4). Consistent with being monomeric, KP insulin also rapidly formed fibrils, with fibrils first detectable at 2 h. The *cis* dicarba KP insulin fibrillation is evident between $t = 6 - 8$ h. Interestingly, the fibrils formed by both *cis*

dicarba insulin and *cis* dicarba KP insulin appeared shorter, thicker and of different morphology to those arising from native insulin and KP insulin (Fig. 4; see *cis* dicarba insulin at t = 15 h and *cis* dicarba KP insulin at t = 8 h). These observations are consistent with the fact that thioflavin T (ThT), a dye commonly used to detect insulin fibrils, did not bind *cis* dicarba insulin fibrils (data not shown). ThT normally binds to insulin fibrils at two sites (between fibers and/or between protofilaments) (38). Our data suggest that while *cis* dicarba insulin is not inherently monomeric it is conformationally different to native insulin.

Cis dicarba insulin and cis dicarba KP insulin are thermodynamically less stable than native insulin – Next, we compared the thermodynamic stability of the *cis* dicarba insulin with the *cis* dicarba KP insulin. Introduction of a dicarba A6-A11 bond into KP insulin also led to a decrease in thermal and chemical denaturation stabilities. The far-UV CD spectra (190 – 260 nm) of Zn^{2+}-free *cis*- and *trans* dicarba KP insulin exhibited lower helical content (34 % and 17 %, respectively) compared to KP insulin (44 %) (see Fig. 5*A* and Table 1). The $[\theta]_{222}$ values are directly proportional to the helical content of the proteins. As seen with the *cis* dicarba insulin (24), the *cis* dicarba KP insulin (Fig. 5*B*) exhibited smaller $[\theta]_{222}$ negative magnitudes measured at 20 °C consistent with their lower initial helical content (Table 1). Denaturation induced by increasing temperature (20 – 70°C) (Fig. 5*B*) or GdnHCl concentrations (0 – 8M) (Fig. 5*C*) was monitored at wavelength 222 nm using CD. The relative thermodynamic stabilities of KP insulins were determined by comparing the relative change of ellipticity with increasing temperature at 1 °C intervals, i.e. by comparing the slope of temperature denaturation curves. Native and KP insulins exhibited similar thermal denaturation curves, whereas the *cis* dicarba KP insulin exhibited relatively small changes in ellipicity due to its significantly lower starting helical content (Fig. 5*B* and Table 1). The *cis* dicarba KP insulin is also considerably less stable upon GdnHCl denaturation, with $\Delta G°_u$ = 1.71 kcal mol^{-1}, as was seen with the dicarba insulin isomers (Fig. 5*C*, Table 1 and (24)).

The effect of introduction of the *cis* dicarba bond on thermodynamic stability is striking and much greater than the introduction of the KP mutation (Fig. 5, *B* and *C*, and (24)). The observed reduction in stability is thus independent of being monomeric.

The cis dicarba A6-A11 linkage promotes a structural change in the B chain helix, which leads to instability – In order to explain why the *cis* dicarba peptides are less thermodynamically stable, we performed a limited proteolysis study that allowed us to detect structural differences between the *cis* dicarba peptides, native insulin and KP insulin. This involved RP-HPLC separation of fragments generated by chymotrypsin proteolysis and subsequent mass spectrometry. Firstly, we observed that *cis*- and *trans* dicarba insulin isomers eluted later (15.8 and 14.6 min, respectively) than native insulin (13.3 min) when separated by RP-HPLC (Fig. 1*D*). Similarly, the *cis*- and *trans* KP isomers also eluted with delayed retention times (16.3 and 15.1 min, respectively) compared to KP insulin (13.5 min) (Fig. 1*E*). The relative delay in the retention times of dicarba insulins is an indication of an apparent increase in hydrophobicity compared to the native forms, with *cis* dicarba insulins being more surface hydrophobic. This was the first indication that the *cis* A6-A11 dicarba linkage induces a more open conformation of insulin than in the native hormone, and that it is likely that hydrophobic residues of the core are more exposed.

The enzymatic stability of dicarba insulin analogues was investigated through limited proteolysis by chymotrypsin under non-reducing conditions. The rate and kinetics of proteolysis were monitored through RP-HPLC as described in the *Experimental Procedures*. Our results show that *cis* dicarba insulin is significantly more rapidly cleaved by chymotrypsin compared to native insulin (Fig. 6*A*). At a protein: enzyme ratio of 86: 0.078 μM, the native insulin remained almost completely undigested after 3 h of proteolysis (> 95 % undigested peptide remaining), whereas almost no intact *cis* dicarba insulin remained. The monomeric KP insulin is more susceptible to proteolysis than insulin with ~ 65% undigested peptide remaining after 3 h (~ 30 % reduction compared to native insulin). However, the *cis* dicarba KP insulin is rapidly cleaved with only ~ 30% of undigested peptide remaining at 3 h (~ 30% reduction compared to KP insulin). As different batches of chymotrypsin were used in the *cis* dicarba insulin and *cis* dicarba KP insulin experiments (Fig. 6*A* *vs* Fig. S4*A*) we cannot determine if the difference in cleavage rates between the two *cis* dicarba analogues is significant. Clearly both are much more rapidly cleaved than native insulin and KP insulin, respectively.

Our RP-HPLC chromatograms of a chymotrypsin-cleaved insulin (Fig. 6B; also see Fig. S3*E*) and the *cis* dicarba insulin (Fig. 6*C*; also see Fig. S3*F*) were comparable to previously reported data, which identified 4 non-reduced metabolites (termed **A**, **B**, **C**, **D**) post-cleavage (39). Through positive ion mode of MALDI mass analysis of the entire digest, we detected native insulin metabolites **A**, **C** and **D** following the chymotrypsin digest (protein: enzyme ratio of 86: 0.078 μM; t = 60 min) but metabolite **B** was not detected (see chromatograms in Figs. 6*B* and S3*E*, MALDI analysis in Fig. S5 and schematic diagram in Fig. S7). By analysis of individual RP-HPLC fractions we could assign the different masses to individual peaks (Fig. S5 and S6; *tables in bottom panel*). Metabolite **A** eluted ≈ 1 min after the undigested peptide (Fig. 6, *B* and *C*), as was seen for all digested insulins (native and dicarba analogues) (*labelled as 2 (grey)* in Figs. S3 and S4, *E* – *G*). Peptides equivalent to metabolite **C** and metabolite **D** eluted at t_R ≈ 3.5 min and ≈ 9.5 min respectively for all insulins (see Fig. 6, *B*, *C* and *F*; labelled as *3* (Metabolite **C**; *orange*) and 4 (Metabolite **D**; *green*) in Figs. S3 and S4, *E* – *G*).

A6-A11 disulfide affects insulin B chain conformation

Close comparison of the RP-HPLC chromatograms revealed the presence of an apparently unique metabolite in chymotrypsin digests of *cis* dicarba insulins (Metabolite **E** in Fig. 6*C*; Metabolite 5, *cis* dicarba KP insulin Fig. S4*F*) that was not detected in native insulin (Fig. 6*B*) or KP insulin (Fig. S4*E*). Metabolite **E** was detected in proteolytic samples of *cis* dicarba insulin as early as t = 1 h (kinetics of cleavage shown in Fig. S3*C* and *F*). Analysis from MALDI data in *negative ion* mode identified the *cis* dicarba insulin metabolite **E** from a fractionated and *reduced* sample (Fig. 6*D*). As shown in the simplified schematic diagram, Figure 6*F (orange box)*, the new metabolite is a full-length two-chain peptide (with intact A6-A11 dicarba bond and A7-B7 and A19-B20 disulfide bonds) with a single cleavage at the *C*-terminal end of Tyr^{B16} of B chain (indicated in *cis* dicarba insulin crystal structure in Fig. 6*E*, *blue circled 1*). This new metabolite **E** was not identified in native insulin (Figs. 6*B*, S3 and S5) or KP insulin (Fig. S4) cleaved with chymotrypsin, suggesting that chymotrypsin is able to access Tyr^{B16} in *cis* dicarba insulin more readily than in insulin or KP insulin.

In order to understand why only *cis* dicarba insulin is cleaved at this new site, we superimposed insulin structures on the active site of chymotrypsin, ensuring that the tyrosine residue that is recognised by the enzyme was localised in the appropriate binding pocket (Fig. 7). Significant steric interactions between the insulin structure and chymotrypsin (Fig. 7*B*) revealed that it would be necessary for the B chain helix of insulin to bend significantly to allow Tyr^{B16} to engage with the chymotrypsin enzyme. Such bending behaviour is evident in our previously reported MD simulations of insulin and its *cis* dicarba analogue (24). It is significant that this bending motion occurs more frequently and persists longer in *cis* dicarba insulin (see below). Hydrogen bonds between Val^{B12} and Tyr^{B16}, Glu^{B13} and Leu^{B17}, and Tyr^{B16} and Gly^{B20} must all be broken, allowing the Cα-Cα distances between Glu^{B13} and Tyr^{B16} and between Tyr^{B16} and Gly^{B20} to increase from their unperturbed values of ~ 5.5 Å to ≥ 7 Å (Fig. 7*A*). This allows Tyr^{B16} to occupy the chymotrypsin binding pocket, with the two neighbouring loops of the helix wrapping around the binding pocket walls (compare Fig. 7*B vs* 7*C*). These changes in the B chain helix structure are concomitant with the twisting of Cys^{B7}, generally resulting in a decrease of the Cα-Cα distance across the A7-B7 disulfide linkage and an increase in its torsional strain. The effects of the bulging in the B chain helix are thereby transmitted to the *N*-terminal helix of the A chain. This results in the *N*-terminal end of this latter helix being tilted away from the B chain helix, although it is important to note that this conformation of the A chain is also seen in the absence of B helix bulging, and also in circumstances when Cys^{B7} is not twisted.

The propensity of the B chain helices of both insulin and the *cis* dicarba insulin to undergo bulging can be assessed through the MD simulation data. In Figure 8, this bulging is monitored *via* the Glu^{B13} - Tyr^{B16} Cα-Cα distance (*green*). The corresponding Cys^{A7} - Cys^{B7} Cα-Cα distances (*purple*) and the strain in the A7-B7 disulfide linkages (*blue*) are also shown. It is clear that, while bending of the B chain helix can occur in both insulin and the *cis* dicarba insulin, it occurs far more frequently in the *cis* dicarba analogue (Fig. 8, *A* and *B*, outlined in black boxes), with the bulging events being more prolonged and showing increased spreading of the loops of the helix (Fig. 7*A*). As noted previously, the A chain *N*-terminal helix is far more labile in the *cis* dicarba insulin than in insulin (24). It appears that in the more stable insulin structure, the A6-A11 disulfide linkage rapidly dampens the bending of the B chain helix and restores its helical structure. In contrast, this conformational lability of αAN in the *cis* dicarba insulin allows the bulge in the B chain helix to form more readily and to persist long enough to allow engagement with and digestion by chymotrypsin. It is important to note that there does not appear to be any correlation between bulging of the B chain and the unwinding motion of the A chain necessary for complexation of the insulin receptor (Fig. S9).

A second important consequence of enhanced B chain bulging for the *cis* dicarba insulin is that the hydrophobic core of the hormone is opened up, resulting in increased exposure to solvent (Fig. 8, *red*). This is consistent with the longer observed elution time of the *cis* analogue in the RP-HPLC experiments (Fig. 1*D*).

In summary, the limited proteolytic-MS integrated analyses revealed that the kinetics of dicarba insulins proteolysis are different from those of native insulin, leading to the formation of new metabolites. This supports the notion that installation of the intra-chain dicarba bridge enhances structural perturbation near Tyr^{B16} to permit access of chymotrypsin to this site.

DISCUSSION

For the last decade, insulin analogue design has focused on improving insulin efficacy and stability. Ideally, we require new rapid-acting insulin analogues that perfectly mimic the normal rapid onset of bolus insulin action. Desirably, insulin analogues would also be physically and chemically stable during pump delivery or at sites of injection. The 'bottleneck' to creating the perfect insulin arises from our incomplete understanding of the relationship between insulin's structure and function, particularly with respect to the fine balance between activity and stability.

Previously, we reported the chemical synthesis of two A6-A11 dicarba insulin analogues (*cis*- and *trans* dicarba insulins). Using these stereoisomers, we obtained remarkable insight into the previously unexplored function of the insulin A6-A11 disulfide bond in modulating insulin activity. Unique to these insulin analogues, only *cis* dicarba insulin is biologically active while *trans* dicarba insulin is inactive. We proposed that the underlying cause of this difference lies in the structural dynamics of the A6-A11 linkage, and that this dictates insulin's ability to transition into its active conformation. We demonstrated that the configuration of the A6-A11

linkage could modulate insulin's ability to engage with the receptor through its influence on the conformational flexibility of the *N*-terminal A chain helix (24).

In the current study, we seek to explain why *in vivo* the *cis* dicarba insulin promotes more rapid lowering of blood glucose than native insulin. Taken together with our observation of reduced thermal and chemical denaturation stabilities we hypothesised the rapid action might be attributed to the *cis* dicarba insulin being monomeric. To address this, we undertook biophysical analyses of the *cis* dicarba insulin in comparison to the *cis* isomer of dicarba KP insulin, which we assume is monomeric as per KP insulin.

We first compared receptor binding and biological activity of the dicarba KP insulins with the *cis*- and *trans* dicarba insulins and native insulin. Consistent with the unique biological characteristics of *cis*- and *trans* dicarba isomers of native insulin, the *cis* dicarba KP insulin was also equipotent to native insulin (receptor binding, receptor activation, DNA synthesis in myoblasts and glucose uptake by adipocytes) while the *trans* dicarba KP insulin was inactive. This confirms the functional role of the native A6-A11 cystine bridge. Even in the context of a disrupted dimer interface induced by the B chain *C*-terminal KP mutation, the A6-A11 bond still influences the ability of insulin to engage with the receptor.

Next, we determined that the *cis* dicarba insulin is not inherently monomeric. The AUC results clearly showed that the distribution of *cis* dicarba insulin into monomeric and dimeric forms under zinc free conditions was similar to that of native insulin. This was surprising and prompted us to further explore the biophysical differences between the *cis* dicarba insulin and native insulin that might account for the more rapid action of the *cis* dicarba analogue.

Further evidence of structural differences between the dicarba insulins and native insulin was provided by our fibrillation assays. The qualitative differences in fibrillation rate and fibril conformation between the *cis* dicarba insulin and native insulin are additional indicators of conformational differences in their structures. It is well established that the movement of the B chain *C*-terminus away from the B chain helix and hydrophobic core promotes fibrillation, as is seen with KP insulin (Fig. 4 and (8,33,40,41)). The AUC results show that the *cis* dicarba insulin is not inherently monomeric, suggesting that the dimer interface is not disrupted, and hence this is not the source of the increased fibrillation rate of the *cis* dicarba insulin. Another key feature of fibril formation is the transition of the A chain *N*-terminal helix to a β-sheet, a process which requires displacement of the A chain away from the B chain helix and from the hormone core (9,33). Therefore, we postulated that *cis* dicarba insulin's increased rate of fibrillation compared to native insulin was likely to be connected to its increased flexibility and altered helicity (more π-like) at the *N*-terminus of the A chain.

However, upon further investigation using limited chymotrypsin proteolysis we were able to detect an unexpected difference in the structure of the B chain between the *cis* dicarba insulin and native insulin. The initial cleavage in the *cis* dicarba insulin occurs at the *C*-terminal end of Tyr^{B16} of B chain. This site is not the first site of cleavage in native insulin (the product was not detected), suggesting that the enzyme is unable to readily access this site in fully intact native insulin; cleavage at Tyr^{B16} only occurs after the molecule has been cleaved at other sites. In the *cis* dicarba insulin, initial cleavage at Tyr^{B16} indicates that chymotrypsin can readily access this site, implying that the *C*-terminal end of the B chain has a tendency to be in a non-native, partially open, or bulged, conformation, thereby allowing enzyme access. Interestingly, this bulged conformation does not affect the ability of the *cis* dicarba insulin to bind the insulin receptor. Previous mutation studies at Tyr^{B16} (e.g. to His or Ala) highlighted the importance of this residue in receptor binding as well as being involved in the dimer interface. Interestingly, the Tyr^{B16}Ala insulin mutant behaves as a monomer on size exclusion chromatography (42).

Previously, MD simulations have captured insulin in both "open" and "wide open (receptor bound)" states (23). In that study, the open state referred to a zipper-like opening from the end of the B chain. This state was also observed in our MD investigations of native insulin and its *cis* dicarba analogue. However, here we additionally observe that simulations of the *cis* dicarba insulin show a significantly enhanced propensity for outward bulging of the B chain helix. This opens up the helix loop between Val^{B12} and Leu^{B17}, exposing Tyr^{B16} for chymotrypsin cleavage (see Fig. 7). Hence, the *cis* dicarba linkage causes two fundamental changes to the dynamics of the insulin structure. On the one hand, it increases the mobility of the A chain *N*-terminal helix, enhancing its ability to engage favourably with the insulin receptor. On the other, it decreases the stability of the overall structure. This is seen in both the destabilisation of the B chain helix, increasing its susceptibility to chymotrypsin digestion, and in an increase in the solvent exposure of the hydrophobic core of insulin, leaving the hormone vulnerable to degradation *via* the formation of fibrils.

Recently Wade *et al* reported that the dicarba substitution of the intra-A-chain disulfide bond of the insulin-like peptide H2 relaxin resulted in significantly reduced stability to enzyme degradation in plasma, despite maintaining the ability to bind relaxin's cognate receptor RXFP1. The mechanisms underlying the instability were not explored. Similar to dicarba insulins, dicarba H2 relaxins also displayed structural differences to the native peptide (43). We postulate that the role of intra-A-chain disulfide bond in regulating peptide stability is conserved across the insulin-relaxin superfamily. However, further investigation is required to confirm this.

The rapid action of both *cis* dicarba insulin and *cis* dicarba KP insulin in lowering blood glucose (in comparison with native insulin) is most likely

explained by the increased mobility of the A chain *N*-terminal helix, as observed in our MD simulations. This enhances the ability of *cis* dicarba insulin to adopt a conformation consistent with IR engagement. By restraining the A6-A11 linkage through introduction of a *cis* dicarba bond, the bioactive conformation of the molecule is favoured, and hence the *in vivo* metabolism of glucose is promoted. It is as yet unclear whether the accompanying destabilisation of the B chain helix also contributes to the enhanced glucose consumption.

In conclusion, through introduction of a non-reducible A6-A11 dicarba bridge of fixed configuration into insulin and KP insulin we reveal the functional and structural roles of this linkage. It not only regulates structural flexibility at the *N*-terminus of the A chain helix, which is necessary for receptor binding, but also influences the frequency at which the B-chain helix "bulges", thereby increasing insulin mimetic's vulnerability to heat, chemical and enzymatic degradation.

Our findings suggest there is potential for the development of ultra-rapid insulin analogues through only minimal manipulation of native insulins or existing insulin analogues. Importantly, this study provides a deeper insight into the function of the A6-A11 bond in regulating the balance between optimal insulin potency and structural stability. We anticipate that this detailed understanding of the structural dynamics of insulin will aid in future design of rapid-acting insulin analogues with improved stability. Defining the determinants of receptor binding (including mechanisms driving necessary A- and B-chain flexibility), stability and fibrillation will allow us to design analogues that permit high affinity binding but avoid instability and fibrillation.

EXPERIMENTAL PROCEDURES

Materials – Actrapid® insulin was purchased from Novo Nordisk Pharmaceuticals Pty Ltd. Humalog® lispro (KP insulin) was obtained from Eli Lilly Australia. Hybridoma cells expressing antibodies specific for the IR alpha subunit (83-7) and the insulin-like growth factor 1 receptor (IGF-1R) α-subunit (24-31) were a kind gift from Prof. K Siddle (44-46). [^{3}H]-Thymidine and Eu-PY20 were purchased from Perkin Elmer Life Sciences. Sequencing grade chymotrypsin was purchased from Promega. The sodium salt of iodoacetic acid (IAA), HPLC grade acetonitrile (CH_3CN) and TFA and DTT were purchased from Sigma-Aldrich (St. Louis, MO, USA). Iodoacetamide (IAM) was a product of Bio-Rad (Hercules, CA, USA). All antibodies were purchased from Cell Signalling Technology (Danvers, MA) unless specified. The matrices for MALDI-TOF-MS (sinapinic acid (SA) and α-cyano-4-hydroxycinnamic acid (HCCA)) were products of Bruker Daltonics (Leipzig, Germany). All other reagents used were analytical grade.

Cell lines and cultures conditions – hIR-A and hIR-B overexpressing cells (R^-IR-A and R^-IR-B, respectively) were constructed as described in (47) using R^-fibroblasts (derived from IGF-1R knockout mouse embryonic fibroblasts) - a kind gift from Professor R. Baserga (Philadelphia, PA)(48). L6 rat skeletal myoblasts overexpressing human IR-A (hIR-A L6) were kindly provided by Dr B.F. Hansen (Novo Nordisk A/S, Denmark) (49). P6 cells (BALB/c3T3 cells overexpressing the human IGF-1R) were from Professor R. Baserga (50). All cells were maintained at 37 °C; 5% CO_2. R^-IR-A, R^-IR-B, hIR-A L6 and P6 cells were maintained in Dulbecco's minimal essential medium (DMEM) High Glucose (4.5 g/mL) supplemented with 10% FCS, 2 mM L-glutamine, 100 U/l penicillin and 100 µg/L streptomycin. All cell culture media and supplements were purchased from Thermo Fisher Scientific Australia.

Chemical synthesis of dicarba insulins – The synthesis of c[Δ^4A6,11]-dicarba insulin (*cis*- and *trans* dicarba insulins) (24) and c[Δ^4A6,11]-dicarba KP insulins (*cis*- and *trans* dicarba KP insulins) were essentially the same. Synthesis of dicarba A chain was achieved through an interrupted solid-phase peptide synthesis (SPPS)-catalysis and ring-closing metathesis (RCM) procedures (24,34). Construction of insulin and KP insulin B-chain was achieved through microwave-accelerated SPPS. The monocyclic A-B conjugates were prepared by combination of the dicarba A chains with the insulin (or KP insulin) B chain under basic conditions resulting in spontaneous oxidation of the liberated free thiol groups generating *cis*- and *trans* dicarba insulins (or *cis*- and *trans* dicarba KP insulins). The details of the synthesis method for the dicarba KP insulins are provided in the *Supporting Information*. The synthesis method for dicarba insulins have been previously described in (24).

Immunocaptured-receptor binding assay – IR-A, IR-B and IGF-1R binding was measured essentially as described by Denley *et al.* (47). Human IR isoform A (IR-A), isoform B (IR-B) and IGF-1R were solubilized from R^-IR-A, R^-IR-B and P6 cells, respectively. Briefly, cells were serum-starved in serum free media (SFM) containing 1% BSA for 4 h before lysis in ice-cold lysis buffer (20 mM HEPES, 150 mM NaCl, 1.5 mM $MgCl_2$, 10% (v/v) glycerol, 1% (v/v) Triton X-100, 1 mM EGTA, and 1 mM phenylmethylsulfonyl fluoride, pH 7.5) for 1 h at 4 °C. Lysates were centrifuged for 10 min at 2,200 × g, then 100 µL lysate was added per well to a white Greiner Lumitrac 600 96-well plate previously coated with anti-IR antibody 83-7 or anti-IGF-1R antibody 24-31 (250 ng/well in bicarbonate buffer pH 9.2). Approximately 500,000 fluorescent counts of europium-labelled insulin (Eu-insulin, prepared in-house) were added to each well along with increasing concentrations of unlabelled competitor in a final volume of 100 µL and incubated for 16 h at 4 °C. Wells were washed four times with 20 mM Tris pH 7.4, 150 mM NaCl and 0.1% (v/v) Tween-20 (TBST). Then 100 µL/well DELFIA enhancement solution (PerkinElmer Life Sciences) was added. After 10 min time-resolved fluorescence was measured using 340 nm excitation and 612 nm emission filters with a BMG Lab Technologies Polarstar fluorometer (Mornington, Australia). Assays were performed in triplicate in at least three independent experiments.

Kinase receptor activation assay (KIRA) – IR-A, IR-B and IGF-1R phosphorylation was detected essentially as described by Denley *et al.* (47). Briefly, R$^-$IR-A, R$^-$IR-B or P6 cells (5×10^4 cells/well) were plated in a 96-well flat bottom plate and grown overnight at 37 °C, 5% CO_2. Cells were serum-starved for 4 h before treatment with insulin or dicarba insulins in 100 µL of SFM / 1% BSA for 10 min or in a time course (0, 2, 5, 8, 12, 20, 30 min) at 37 °C, 5 % CO_2. Cells were lysed with ice-cold lysis buffer containing 2 mM Na_3VO_4 and 100 mM NaF, and receptors were captured onto white Greiner Lumitrac 600 96-well plates pre-coated with anti-IR antibody 83-7 or anti-IGF-IR antibody 24-31 (250 ng/well) (44) and blocked with 20 mM Tris-HCl pH 7.4, 150 mM NaCl, and 0.1% (v/v) Tween-20 (TBST) / 0.5% BSA. Following overnight incubation at 4 °C, the plates were washed three times with TBST. Phosphorylated receptor was detected by incubation with Eu-PY20 (76 ng/well) at room temperature for 2 h. Wells were washed four times with TBST, and time-resolved fluorescence was detected as described above. Assays were performed in triplicate in at least three independent experiments.

DNA synthesis assay – DNA synthesis was carried out as described in Gaugin *et al.* (51). Briefly, hIR-A L6 myoblasts were plated in a 96-well flat bottom plate (1.5×10^4 cells/well) and grown overnight at 37 °C, 5% CO_2. Cells were starved in SFM / 1% BSA for 4 h before treatment with increasing ligand concentrations for 18 h in SFM / 1% BSA. The cells were incubated with 0.13 µCi/well [^{3}H]-thymidine for 4 h, shaken for 2 h with 50 µL disrupting buffer (40mM Tris pH 7.5, 10mM EDTA and 150 mM NaCl) and then harvested onto glass fibre filters (Millipore®) using a MICRO 96.™ Skatron harvester (Molecular Devices). The filters were counted in a Wallac MicroBeta counter (PerkinElmer Life Sciences). Assays were performed in triplicate in at least three independent experiments.

Glucose uptake assay – Briefly, NIH3T3-L1 myoblasts (up to passage 20) grown in DMEM supplemented with 10 % newborn calf serum, 2mM L-glutamine, 100 U/l penicillin and 100 µg/L streptomycin at 37 °C were seeded into 24-well plates at 5 x 10^3 cells/well and grown for 8 days to confluence and were then differentiated into adipocytes as described (52). Glucose uptake in response to insulin and dicarba insulin analogues was measured essentially as described (53). Briefly, 3T3-L1 adipocytes were serum starved in SFM / 1% BSA for 4 h, washed twice with Krebs-Ringer phosphate buffer (KRP; 12.5 mM HEPES, 120 mM NaCl, 6 mM KCl, 1.2 mM $MgSO_4$, 1 mM $CaCl_2$, 0.4 mM Na_2HPO_4 and 0.6 mM Na_2HPO_4 (pH7.4)) containing 1% BSA and incubated for 15 min at 37 °C. Insulin or insulin analogues was added at decreasing concentrations (100 – 0.3 nM) for 30 min at 37 °C. For the final 10 min, 2-deoxyglucose (2-DOG) uptake was initiated by the addition of 50 µM *cold* deoxyglucose and 1 µCi [^{3}H]-deoxyglucose per well. The assay was terminated by rapidly washing the cells three times with ice-cold KRP buffer. Cells were solubilized in 0.5 M NaOH / 0.1% SDS and ^{3}H content was determined by scintillation counting. Non-specific 2-DOG uptake was determined in the presence of 50 µM cytochalasin B.

Insulin tolerance test – Eight-week-old C57BL6 male mice were fed either a standard rodent chow diet containing (wt/wt) 77% carbohydrate, 20% protein, and 3% fat from Ridley AgriProducts (Pakenham, Victoria, Australia) or a high fat diet (HFD) containing (wt/wt) 57 % carbohydrate, 19% protein and 15% fat from Specialty Feeds (SF08-044, Glen Forrest, Western Australia, Australia) for 12 weeks. Mice (5 or 6 mice per group) were injected *ip* with 0.75I U/kg insulin or insulin analogues under non-fasting conditions and tail vein blood glucose was measured *via* glucometer at indicated times (54). Experimental procedures were carried out in accordance to the protocols approved by the Austin Health Animal Ethics Committee (AEC 2011/04396). Native insulin (Actrapid) and KP insulin (Humalog) were administered as formulated peptide diluted to the correct dose in phosphate-buffered saline pH 7.4 (semi-formulated). Both *cis* dicarba insulin and *cis* KP dicarba insulin were dissolved in 10mM HCl and diluted to the correct dose in phosphate-buffered saline pH 7.4 (non-formulated). Subsequent to this experiment we found no difference between semi-formulated KP insulin and non-formulated KP insulin in an insulin tolerance test (Fig. S10), demonstrating that the vehicles had no effect on the insulin tolerance test outcomes.

Sedimentation equilibrium analytical ultracentrifugation (SE-AUC) – Analytical ultracentrifugation was conducted at 20 °C using a Beckman XLI analytical centrifuge in 12 mm path-length cells. *Cis* dicarba insulin was diluted from a 10 mg / ml stock in 10 mM HCl into 100 µL 10 mM sodium phosphate, 100 mM NaCl, pH 7.4, with or without 0.2 mM $ZnCl_2$ to a final concentration of 100 or 300 µg/mL. Radial concentration distributions were measured by absorbance at 230 nm. Sedimentation equilibrium was established at 25,000 and 40,000 rpm, as assessed by sequential absorbance scans 2 h apart. Data at both speeds were jointly fit to a single ideal sedimenting species or to various models of self-association in SEDPHAT (55), using values of solution density and solute partial specific volume estimated from composition using SEDNTERP (56), neglecting any effect of the dicarba modification. Mass conservation was applied as a constraint on the fits by floating the position of the bottom of the cell. Reported errors describe the precision of the fit at 0.68 confidence level, estimated from Monte Carlo simulations as implemented in SEDPHAT.

Atomic force microscopy (AFM) – Analysis of fibrillation was monitored by AFM essentially as described (57). Briefly, lyophilized insulin, insulin lispro and dicarba isomers were re-suspended in 200 mM KCl-HCl in Milli-Q water, pH 1.6 at 200 µM (1.16 mg/mL) and incubated at 60 °C with gentle agitation. Samples (5 µL) were taken at different times, diluted 1: 10 in the same buffer and immediately frozen. 30 µL of the insulin solution was dropped onto

a freshly cleaved mica substrate. Once dried, the sample was washed dropwise with Milli-Q water, and then dried with a gentle stream of dry nitrogen. Images of the protein aggregates were recorded with a Multimode Nanoscope IV Atomic Force Microscope (Veeco Instruments, Santa Barbara, CA, USA), operating in Tapping Mode. Rigid cantilevers with resonance frequencies of 325 kHz and equipped with silicon tips (Mikromasch HQ: NSC15, Bulgaria) with nominal spring constant of 40 N/m and a nominal tip diameter of 16 nm were used. Typical scan size was 5 µm (512×512 points), and scan rate was 1-2 Hz. The scanner was calibrated in the x, y and z axes using silicon calibration grids (Bruker model numbers PG: 1 µm pitch, 110 nm depth and VGRP: 10 µm pitch, 180 nm depth). Images were analysed using the Nanoscope analysis program version 1.40.

Reversed-phase High Performance Liquid Chromatography (RP-HPLC) – Purification of insulin analogues was performed on a Vydac C_4 analytical column (214TP5210; 5 µm, 2.1 x 100 mm, 300 Å) connected to the Agilent 1260 Infinity Quaternary LC system. Buffer A: 0.1% aqueous TFA. Buffer B: 80% CH_3CN in 0.08% TFA. Peptides were eluted using a linear gradient of 20 – 25 % CH_3CN for 5 min, followed by a 25 – 38 % CH_3CN gradient over 13 min at flow rate of 0.5 mL/min. UV detection was at 280 nm and peak areas were used for quantitation of peptides.

Circular Dichroism (CD) – CD was carried out as previously described (24). Briefly, CD spectra were recorded on a Jasco J-815 CD spectrometer. Spectra were from 260 to 190 nm with a 1.0 nm step size using a 1.0 s response time and 1.0 nm bandwidth in a quartz cuvette with a 0.1 cm path length. Insulin and insulin analogues were incubated in 10 mM phosphate buffer (pH 7.4) to a concentration of 0.22 mg/mL (38 µM). Spectra were background-corrected by subtraction of the spectrum of buffer alone. Temperature denaturation was achieved by automated thermal control increasing by 2 °C / min at 1 °C intervals. Samples were diluted to 10 µM for equilibrium denaturation studies in guanidine hydrochloride (GdnHCl) (1 – 8 M). The machine unit collected, θ in millidegrees, is converted to mean residue ellipicity (MRE), [θ] in degrees.cm^{2}dmol^{-1}residue^{-1}, as follows:

$$[\theta] = \theta \times \frac{(0.1 \times MRW)}{(P \times Conc.)}$$

where MRW is the protein mean weight ((atomic mass units/daltons) / number of residues)), P is pathlength (cm) and Conc. is protein concentration in mg/mL. $[\theta]_{222}$ is the molar ellipicity per residue at wavelength 222 nm.

In-solution Time-course Limited Proteolysis Assay – Limited proteolysis analyses were performed in 100 mM Tris-HCl pH 7.5 using sequencing grade chymotrypsin at final protease: peptide ratio of 1: 50 or 1: 250 (w/w); incubated at 37 °C. The final concentration of peptide was 0.5 mg/mL. The proteolytic reactions were analysed on a time-course basis by sampling 10 µL of proteolytic mixture (equivalent to 5 µg of insulin) into 100 µL 0.5% (v/v) TFA at t = 0, 1, 2 and 3 h. Digested samples were analysed and fractionated (fraction size: 0.25 mL or 0.5 mL) using RP-HPLC and lyophilised. The extents of proteolysis were analysed as follows:

$$\%\ of\ Undigested\ Peptide = \frac{Mass\ of\ Undigested\ Peptide\ at\ T = x}{Mass\ of\ Undigested\ Peptide\ at\ T = 0}\ x\ 100\ \%$$

Preparation of proteolysed insulins samples for mass spectrometry – Lyophilised fractions were resuspended in 20 µL of 100 mM ammonium bicarbonate (NH_4HCO_3). Half of the volume was kept separately as *non-reducing* samples for mass spectrometry analysis. The other half was *reduced* in 5 mM DTT for 45 min at 56 °C and alkylated with 14 mM IAM (for positive mode) or IAA (for negative mode) for 30 minutes in the dark at room temperature.

Matrix-Assisted Laser Desorption and Ionization Time-of-Flight Mass Spectrometry (MALDI-TOF MS) analysis – The molecular weights of intact insulin analogues and the proteolytically cleaved metabolites were identified using MALDI-TOF Autoflex™ III (Bruker Daltonics, Leipzig, Germany) equipped with a Nd: YAG laser (wavelength: 355nm). Either the entire cleavage mixture or isolated peaks separated by RP-HPLC were subjected to mass spectral analysis using combinations of positive or negative ion with linear or reflectron mode. Insulin digest samples intended for mass analysis using positive mode were desalted using Zip-Tip C_{18} (Millipore®, Billerica, MA, USA), eluted with 2 µL of 0.1 % TFA / CH_3CN (70: 30, v/v). Samples intended for negative mode analysis were desalted and eluted with no TFA. 1 µL of each sample was spotted onto the MTP 384 ground steel target plate (Bruker Daltonics), air dried, then 1 µL of SA matrix is spotted on top of each dried sample. Calibrations were performed using Bruker Daltonics' Peptide Calibration Standard II and Protein Calibration Standard I according to manufacturer's instructions.

Molecular Dynamics, MD – Previously, MD simulations of insulin and its *cis* dicarba analogue were performed, and the different behaviours of the *N*-terminal A chain helix analysed in detail (24). Here, these simulation data are further analysed to give insight into the effect of the A6-A11 linkage on insulin structural stability. Details of the simulation and analysis protocols are provided in our previous report (24), and in the Supplementary Material. In brief, the AMBER14 program package (58) in conjunction with *Amber ff14SB force field parameters*(59) (along with calculated parameters for the dicarba linkage) were used to perform 200 ns room-temperature MD simulations for insulin and its dicarba isomers based on four different starting structures derived from high-resolution X-ray crystallography experiments. Twelve independent 200 ns simulations were performed for insulin and 16 simulations for the *cis* dicarba insulin. Simulation frames recorded at 200 ps intervals were used for the analysis in this paper (1000 frames per

simulation). Data were processed and analysed using CPPTRAJ, (60) along with custom computer scripts. The torsional strain in the A7-B7 disulfide linkages was estimated based on the data reported in references (61,62). Insulin structures were superimposed on the crystal structure of a chymotrypsin-inhibitor complex (PDB: 4h4f) using Swiss-PDBViewer (63) and VMD (64).

Statistical Analyses – Statistical analysis of receptor binding, receptor activation and DNA synthesis assays were performed using a 2-way ANOVA with a Dunnett's multiple comparison. Insulin tolerance test and glucose uptake assay data were analysed with a paired *t*-test. Significance was accepted at $P < 0.05$.

Acknowledgements: We thank Dr Daniel Jardine and Jason Young for providing training on MALDI analysis (Flinders Analytical of Flinders University) and Dr Christopher Gibson (Scanned Probe facility, Flinders University) for AFM technical assistance. Simulations were performed using high performance computing resources provided by the Victorian Partnership of Advanced Computing (access funded by Deakin University) and the National Computational Infrastructure (NCI) Facility, which is supported by the Australian Government.

Conflict of interest: none

Author contributions: SCO performed in vitro activity assays, biophysical analyses and mass spectrometry analysis. AB and BVL conducted chemical syntheses, CAM and RSN performed the ultracentrifugation assay, CD performed the AFM assay, SA performed the insulin tolerance test, NLH conducted the MD analyses. AJR and BEF conceived and coordinated the study. SCO, RSN, NLH, AJR and BEF wrote the paper. All authors reviewed and approved the final version of manuscript.

REFERENCES

1. Banting, F. G., and Best, C. H. (2007) The internal secretion of the pancreas. 1922. *Indian J. Med. Res.* **125**, 251-266
2. Pandyarajan, V., and Weiss, M. A. (2012) Design of non-standard insulin analogs for the treatment of diabetes mellitus. *Curr. Diab. Rep.* **12**, 697-704
3. Mathieu, C., Gillard, P., and Benhalima, K. (2017) Insulin analogues in type 1 diabetes mellitus: getting better all the time. *Nat. Rev. Endocrinol.* **13**, 385-399
4. Adams, M. J., Blundell, T. L., Dodson, E. J., Dodson, G. G., Vijayan, M., Baker, E. N., Harding, M. M., Hodgkin, D. C., Rimmer, B., and Sheat, S. (1969) Structure of Rhombohedral 2 Zinc Insulin Crystals. *Nature* **224**, 491-495
5. Weiss, M. A. (2009) The structure and function of insulin: decoding the TR transition. *Vitam. Horm.* **80**, 33-49
6. De Meyts, P. (2015) Insulin/receptor binding: the last piece of the puzzle? What recent progress on the structure of the insulin/receptor complex tells us (or not) about negative cooperativity and activation. *Bioessays* **37**, 389-397
7. Brange, J., and Langkjoer, L. (1993) Insulin structure and stability. *Pharm. Biotechnol.* **5**, 315-350
8. Hua, Q. X., and Weiss, M. A. (2004) Mechanism of insulin fibrillation: the structure of insulin under amyloidogenic conditions resembles a protein-folding intermediate. *J. Biol. Chem.* **279**, 21449-21460
9. Yang, Y., Petkova, A., Huang, K., Xu, B., Hua, Q. X., Ye, I. J., Chu, Y. C., Hu, S. Q., Phillips, N. B., Whittaker, J., Ismail-Beigi, F., Mackin, R. B., Katsoyannis, P. G., Tycko, R., and Weiss, M. A. (2010) An Achilles' heel in an amyloidogenic protein and its repair: insulin fibrillation and therapeutic design. *J. Biol. Chem.* **285**, 10806-10821
10. Ciszak, E., Beals, J. M., Frank, B. H., Baker, J. C., Carter, N. D., and Smith, G. D. (1995) Role of C-terminal B-chain residues in insulin assembly: the structure of hexameric LysB28ProB29-human insulin. *Structure* **3**, 615-622
11. Campbell, R. K., Campbell, L. K., and White, J. R. (1996) Insulin lispro: its role in the treatment of diabetes mellitus. *Ann. Pharmacother.* **30**, 1263-1271
12. Ludwig, D. B., Webb, J. N., Fernández, C., Carpenter, J. F., and Randolph, T. W. (2011) Quaternary conformational stability: The effect of reversible self-association on the fibrillation of two insulin analogs. *Biotechnol. Bioeng.* **108**, 2359-2370
13. Woods, R. J., Alarcón, J., McVey, E., and Pettis, R. J. (2012) Intrinsic Fibrillation of Fast-Acting Insulin Analogs. *J. Diabetes Sci. Technol.* **6**, 265-276
14. Lawrence, M. C., and Ward, C. W. (2015) Structural Features of the Receptor Tyrosine Kinase Ectodomains. in *Receptor Tyrosine Kinases: Structure, Functions and Role in Human Disease* (Wheeler, D. L., and Yarden, Y. eds.), Springer New York, New York, NY. pp 163-193
15. Menting, J. G., Whittaker, J., Margetts, M. B., Whittaker, L. J., Kong, G. K., Smith, B. J., Watson, C. J., Zakova, L., Kletvikova, E., Jiracek, J., Chan, S. J., Steiner, D. F., Dodson, G. G., Brzozowski, A. M., Weiss, M. A., Ward, C. W., and Lawrence, M. C. (2013) How insulin engages its primary binding site on the insulin receptor. *Nature* **493**, 241-245
16. Jensen, M. (2000) *Analysis of structure-activity relationships at the insulin molecule by alanine-scaning mutagenesis.*Master Thesis, University of Copenhagen
17. Whittaker, L., Hao, C., Fu, W., and Whittaker, J. (2008) High-affinity insulin binding: insulin interacts with two receptor ligand binding sites. *Biochemistry* **47**, 12900-12909
18. Zoete, V., Meuwly, M., and Karplus, M. (2004) A comparison of the dynamic behavior of monomeric and dimeric insulin shows structural rearrangements in the active monomer. *J. Mol. Biol.* **342**, 913-929
19. Zoete, V., Meuwly, M., and Karplus, M. (2005) Study of the insulin dimerization: binding free energy calculations and per-residue free energy decomposition. *Proteins* **61**, 79-93
20. Baker, E. N., Blundell, T. L., F. R. S., Cutfield, J. F., Cutfield, S. M., Dodson, E. J., Dodson, G. G., Hodgkin, D. M., F. R. S., Hubbard, R. E., Isaacs, N. W., Reynolds, C. D., Sakabe, K., Sakabe, N., and Vijayan, N. M. (1988) The structure of 2Zn pig insulin crystals at 1.5 A resolution. *Philos. Trans. R. Soc. Lond. B. Biol. Sci.* **319**, 369-456

21. Menting, J. G., Yang, Y., Chan, S. J., Phillips, N. B., Smith, B. J., Whittaker, J., Wickramasinghe, N. P., Whittaker, L. J., Pandyarajan, V., Wan, Z. L., Yadav, S. P., Carroll, J. M., Strokes, N., Roberts, C. T., Jr., Ismail-Beigi, F., Milewski, W., Steiner, D. F., Chauhan, V. S., Ward, C. W., Weiss, M. A., and Lawrence, M. C. (2014) Protective hinge in insulin opens to enable its receptor engagement. *Proc. Natl. Acad. Sci. U.S.A.*
22. Hua, Q. X., Shoelson, S. E., Kochoyan, M., and Weiss, M. A. (1991) Receptor binding redefined by a structural switch in a mutant human insulin. *Nature* **354**, 238-241
23. Papaioannou, A., Kuyucak, S., and Kuncic, Z. (2015) Molecular Dynamics Simulations of Insulin: Elucidating the Conformational Changes that Enable Its Binding. *PLoS One* **10**, e0144058
24. van Lierop, B., Ong, S. C., Belgi, A., Delaine, C., Andrikopoulos, S., Haworth, N. L., Menting, J. G., Lawrence, M. C., Robinson, A. J., and Forbes, B. E. (2017) Insulin in motion: The A6-A11 disulfide bond allosterically modulates structural transitions required for insulin activity. *Sci. Rep.* **7**, 17239
25. Zakova, L., Kazdova, L., Hanclova, I., Protivinska, E., Sanda, M., Budesinsky, M., and Jiracek, J. (2008) Insulin analogues with modifications at position B26. Divergence of binding affinity and biological activity. *Biochemistry* **47**, 5858-5868
26. Zakova, L., Barth, T., Jiracek, J., Barthova, J., and Zorad, S. (2004) Shortened insulin analogues: marked changes in biological activity resulting from replacement of TyrB26 and N-methylation of peptide bonds in the C-terminus of the B-chain. *Biochemistry* **43**, 2323-2331
27. Chang, S. G., Choi, K. D., Jang, S. H., and Shin, H. C. (2003) Role of disulfide bonds in the structure and activity of human insulin. *Mol. Cells* **16**, 323-330
28. Dai, Y., and Tang, J. G. (1996) Characteristic, activity and conformational studies of [A6-Ser, A11-Ser]-insulin. *Biochim. Biophys. Acta* **1296**, 63-68
29. Hua, Q. X., Jia, W., Frank, B. H., Phillips, N. F., and Weiss, M. A. (2002) A protein caught in a kinetic trap: structures and stabilities of insulin disulfide isomers. *Biochemistry* **41**, 14700-14715
30. Sieber, P., Eisler, K., Kamber, B., Riniker, B., Rittel, W., Marki, F., and de Gasparo, M. (1978) Synthesis and biological activity of two disulphide bond isomers of human insulin: [A7-A11,A6-B7-cystine]- and [A6-A7,A11-B7-cystine]insulin (human). *Hoppe Seyler's Z. Physiol. Chem.* **359**, 113-123
31. Hua, Q.-X., Gozani, S. N., Chance, R. E., Hoffmann, J. A., Frank, B. H., and Weiss, M. A. (1995) Structure of a protein in a kinetic trap. *Nat. Struct. Mol. Biol.* **2**, 129-138
32. Liu, Y., Wang, Z. H., and Tang, J. G. (2004) Flexibility exists in the region of [A6-A11, A7-B7] disulfide bonds during insulin precursor folding. *J Biochem* **135**, 1-6
33. Hua, Q. X., Jia, W., and Weiss, M. A. (2011) Conformational dynamics of insulin. *Front. Endocrinol.* **2**, 48
34. van Lierop, B., Bornschein, C., Roy Jackson, W., and Robinson, A. (2011) Ring-closing Metathesis in Peptides – the Sting is in the Tail! *Aust. J. Chem.* **64**, 806
35. Milthorpe, B. K., Nichol, L. W., and Jeffrey, P. D. (1977) The polymerization pattern of zinc(II)-insulin at pH 7.0. *Biochim Biophys Acta* **495**, 195-202
36. Menting, J. G., Gajewiak, J., MacRaild, C. A., Chou, D. H., Disotuar, M. M., Smith, N. A., Miller, C., Erchegyi, J., Rivier, J. E., Olivera, B. M., Forbes, B. E., Smith, B. J., Norton, R. S., Safavi-Hemami, H., and Lawrence, M. C. (2016) A minimized human insulin-receptor-binding motif revealed in a Conus geographus venom insulin. *Nat Struct Mol Biol* **23**, 916-920
37. Jeffrey, P. D., Milthorpe, B. K., and Nichol, L. W. (1976) Polymerization pattern of insulin at pH 7.0. *Biochemistry* **15**, 4660-4665
38. Groenning, M., Norrman, M., Flink, J. M., van de Weert, M., Bukrinsky, J. T., Schluckebier, G., and Frokjaer, S. (2007) Binding mode of Thioflavin T in insulin amyloid fibrils. *J. Struct. Biol.* **159**, 483-497
39. Schilling, R. J., and Mitra, A. K. (1991) Degradation of insulin by trypsin and alpha-chymotrypsin. *Pharm. Res.* **8**, 721-727
40. Phillips, N. B., Whittaker, J., Ismail-Beigi, F., and Weiss, M. A. (2012) Insulin fibrillation and protein design: topological resistance of single-chain analogs to thermal degradation with application to a pump reservoir. *J. Diabetes Sci. Technol.* **6**, 277-288

41. Brange, J., Andersen, L., Laursen, E. D., Meyn, G., and Rasmussen, E. (1997) Toward understanding insulin fibrillation. *J. Pharm. Sci.* **86**, 517-525
42. Chen, Y., You, Y., Jin, R., Guo, Z. Y., and Feng, Y. M. (2004) Sequences of B-chain/domain 1-10/1-9 of insulin and insulin-like growth factor 1 determine their different folding behavior. *Biochemistry* **43**, 9225-9233
43. Hossain, M. A., Haugaard-Kedstrom, L. M., Rosengren, K. J., Bathgate, R. A., and Wade, J. D. (2015) Chemically synthesized dicarba H2 relaxin analogues retain strong RXFP1 receptor activity but show an unexpected loss of in vitro serum stability. *Org Biomol Chem* **13**, 10895-10903
44. Soos, M. A., and Siddle, K. (1989) Immunological relationships between receptors for insulin and insulin-like growth factor I. Evidence for structural heterogeneity of insulin-like growth factor I receptors involving hybrids with insulin receptors. *Biochem. J.* **263**, 553-563
45. Soos, M. A., O'Brien, R. M., Brindle, N. P., Stigter, J. M., Okamoto, A. K., Whittaker, J., and Siddle, K. (1989) Monoclonal antibodies to the insulin receptor mimic metabolic effects of insulin but do not stimulate receptor autophosphorylation in transfected NIH 3T3 fibroblasts. *Proc. Natl. Acad. Sci. U.S.A.* **86**, 5217-5221
46. Ganderton, R. H., Stanley, K. K., Field, C. E., Coghlan, M. P., Soos, M. A., and Siddle, K. (1992) A monoclonal anti-peptide antibody reacting with the insulin receptor beta-subunit. Characterization of the antibody and its epitope and use in immunoaffinity purification of intact receptors. *Biochem. J.* **288 (Pt 1)**, 195-205
47. Denley, A., Bonython, E. R., Booker, G. W., Cosgrove, L. J., Forbes, B. E., Ward, C. W., and Wallace, J. C. (2004) Structural determinants for high-affinity binding of insulin-like growth factor II to insulin receptor (IR)-A, the exon 11 minus isoform of the IR. *Mol. Endocrinol.* **18**, 2502-2512
48. Sell, C., Dumenil, G., Deveaud, C., Miura, M., Coppola, D., DeAngelis, T., Rubin, R., Efstratiadis, A., and Baserga, R. (1994) Effect of a null mutation of the insulin-like growth factor I receptor gene on growth and transformation of mouse embryo fibroblasts. *Mol. Cell Biol.* **14**, 3604-3612
49. Bonnesen, C., Nelander, G. M., Hansen, B. F., Jensen, P., Krabbe, J. S., Jensen, M. B., Hegelund, A. C., Svendsen, J. E., and Oleksiewicz, M. B. (2010) Synchronization in G0/G1 enhances the mitogenic response of cells overexpressing the human insulin receptor A isoform to insulin. *Cell Biol. Toxicol.* **26**, 293-307
50. Pietrzkowski, Z., Lammers, R., Carpenter, G., Soderquist, A. M., Limardo, M., Phillips, P. D., Ullrich, A., and Baserga, R. (1992) Constitutive expression of insulin-like growth factor 1 and insulin-like growth factor 1 receptor abrogates all requirements for exogenous growth factors. *Cell Growth Differ.* **3**, 199-205
51. Gauguin, L., Delaine, C., Alvino, C. L., McNeil, K. A., Wallace, J. C., Forbes, B. E., and De Meyts, P. (2008) Alanine scanning of a putative receptor binding surface of insulin-like growth factor-I. *J. Biol. Chem.* **283**, 20821-20829
52. Govers, R., Coster, A. C., and James, D. E. (2004) Insulin increases cell surface GLUT4 levels by dose dependently discharging GLUT4 into a cell surface recycling pathway. *Mol. Cell Biol.* **24**, 6456-6466
53. van Dam, E. M., Govers, R., and James, D. E. (2005) Akt activation is required at a late stage of insulin-induced GLUT4 translocation to the plasma membrane. *Mol. Endocrinol.* **19**, 1067-1077
54. Wong, N., Fam, B. C., Cempako, G. R., Steinberg, G. R., Walder, K., Kay, T. W., Proietto, J., and Andrikopoulos, S. (2011) Deficiency in interferon-gamma results in reduced body weight and better glucose tolerance in mice. *Endocrinology* **152**, 3690-3699
55. Houtman, J. C. D., Brown, P. H., Bowden, B., Yamaguchi, H., Appella, E., Samelson, L. E., and Schuck, P. (2007) Studying multisite binary and ternary protein interactions by global analysis of isothermal titration calorimetry data in SEDPHAT: application to adaptor protein complexes in cell signaling. *Protein Science* **16**, 30-42
56. Laue, T., Shah, D., Ridgeway, T., and Pelletier, S. (1992) Computer-aided interpretation of analytical sedimentation data for proteins. in *Analytical Ultracentrifugation in Biochemistry*

and Polymer Science (Harding, S., Rowe, A., and Horton, J. eds.), Royal Society of Chemistry, Cambridge, UK. pp 90-125

57. Manno, M., Craparo, E. F., Podesta, A., Bulone, D., Carrotta, R., Martorana, V., Tiana, G., and San Biagio, P. L. (2007) Kinetics of different processes in human insulin amyloid formation. *J. Mol. Biol.* **366**, 258-274
58. Case, D. A., Babin, V., Berryman, J. T., Betz, R. M., Cai, Q., Cerutti, D. S., Cheatham III, T. E., Darden, T. A., Duke, R. E., Gohlke, H., Goetz, A. W., Gusarov, S., Homeyer, N., Janowski, P., Kaus, J., Kolossváry, I., Kovalenko, A., Lee, T. S., LeGrand, S., Luchko, T., Luo, R., Madej, B., Merz, K. M., Paesani, F., Roe, D. R., Roitberg, A., Sagui, C., Salomon-Ferrer, R., Seabra, G., Simmerling, C. L., Smith, W., Swails, J., Walker, R. C., Wang, J., Wolf, R. M., Wu, X., and Kollman, P. A. (2014) AMBER 14, University of California, San Francisco
59. Maier, J. A., Martinez, C., Kasavajhala, K., Wickstrom, L., Hauser, K. E., and Simmerling, C. (2015) ff14SB: Improving the Accuracy of Protein Side Chain and Backbone Parameters from ff99SB. *J. Chem. Theory Comput.* **11**, 3696-3713
60. Roe, D. R., and Cheatham, T. E., 3rd. (2013) PTRAJ and CPPTRAJ: Software for Processing and Analysis of Molecular Dynamics Trajectory Data. *J. Chem. Theory Comput.* **9**, 3084-3095
61. Haworth, N. L., Liu, J. Y., Fan, S. W., Gready, J. E., and Wouters, M. A. (2010) Estimating relative disulfide energies: an accurate *ab initio* potential energy surface. *Aust. J. Chem.* **63**, 379-387
62. Haworth, N. L., Gready, J. E., George, R. A., and Wouters, M. A. (2007) Evaluating the stability of disulfide bridges in proteins: A torsional potential energy surface for diethyl disulfide. *Mol. Simul.* **33**, 475-485
63. Guex, N., and Peitsch, M. C. (1997) SWISS-MODEL and the Swiss-PdbViewer: An environment for comparative protein modeling. *Electrophoresis* **18**, 2714-2723
64. Humphrey, W., Dalke, A., and Schulten, K. (1996) VMD - Visual Molecular Dynamics. *J. Molec. Graphics* **14**, 33-38

FOOTNOTES

This article contains supporting materials and methods, Table S1and Figs. S1-S11.

[1] SCO and BVL acknowledge the financial support from the Australian postgraduate scholarships.

[2] RSN acknowledges fellowship support from the Australian National Health and Medical Research Council.

[3] AJR and BEF acknowledge funding from the National Health and Medical Research Council (Project Grant APP1069328) and Australian Research Council (LP12020200792).

[4] The abbreviations used are: KP insulin, insulin analogue containing reversed amino acids of $Pro^{B28}Lys^{B29} \rightarrow Lys^{B28}Pro^{B29}$; IR, insulin receptor; C=C or dicarba, unsaturated carbon-carbon bond; S-S bond, disulfide bond, T1D, type 1 diabetes; T2D, type 2 diabetes, αCT, *C*-terminus of the IR alpha chain; L1, leucine-rich repeat domain of IR (residues 1-157); IAA, iodoacetic acid; IAM, iodoacetamide; CH_3CN, acetonitrile; SA, sinapinic acid; HCCA, α-cyano-4-hydroxycinnamic acid; R^- fibroblasts, IGF-1R knockout mouse embryonic fibroblasts; hIR-A or hIR-B, human insulin receptor exon 11- or exon 11+ isoform; IGF-1R, insulin-like growth factor 1 receptor; hIR-A L6, L6 rat skeletal myoblasts overexpressing human IR-A; DMEM, Dulbecco's minimal essential medium; FCS, fetal calf serum; SPPS, solid-phase peptide synthesis; RCM, ring-closing metathesis; SFM, serum-free media; Eu, europium; TBST, tris-buffered saline containing 0.1% (v/v) Tween 20; KIRA, kinase receptor activation assay; PY20, anti-phosphotyrosine antibody; KRP, Krebs-Ringer phosphate buffer; *ip*, intraperitoneal injection; 2-DOG, 2-deoxyglucose; HFD, high-fat diet; AFM, atomic force microscopy; GdnHCl, guanidine hydrochloride; MD, molecular dynamics; SE-AUC, Sedimentation equilibrium analytical ultracentrifugation; *t*, time; t_R, retention time; [CME], carboxymethylcystine.

TABLES

Table 1. Structural analyses of insulin, KP insulin and dicarba insulins using circular dichroism. Helical content calculated using the CONTINLL algorithm for deconvolution against the protein database reference set SP43. The program is available on the DICROWEB website (http://dichroweb.cryst.bbk.ac.uk/html/home.shtml). ΔG° values were derived from guanidine denaturation studies. †Data previously reported in (24).

Analogues	Secondary Structures Content (%)				Guanidine Denaturation
	Helix	Sheet	Turn	Unordered	$\Delta G°_U$ (kcal.mole^{-1})
Insulin†	48%	12%	14%	26%	4.74
***Cis* dicarba insulin**†	37%	16%	20%	27%	1.98
***Trans* dicarba insulin**†	23%	24%	22%	31%	1.61
KPinsulin	44%	14%	14%	28%	n.a.
***Cis* dicarba KP insulin**	34%	19%	20%	27%	1.71
***Trans* dicarba KP insulin**	17%	31%	22%	30%	n.a.

FIGURES

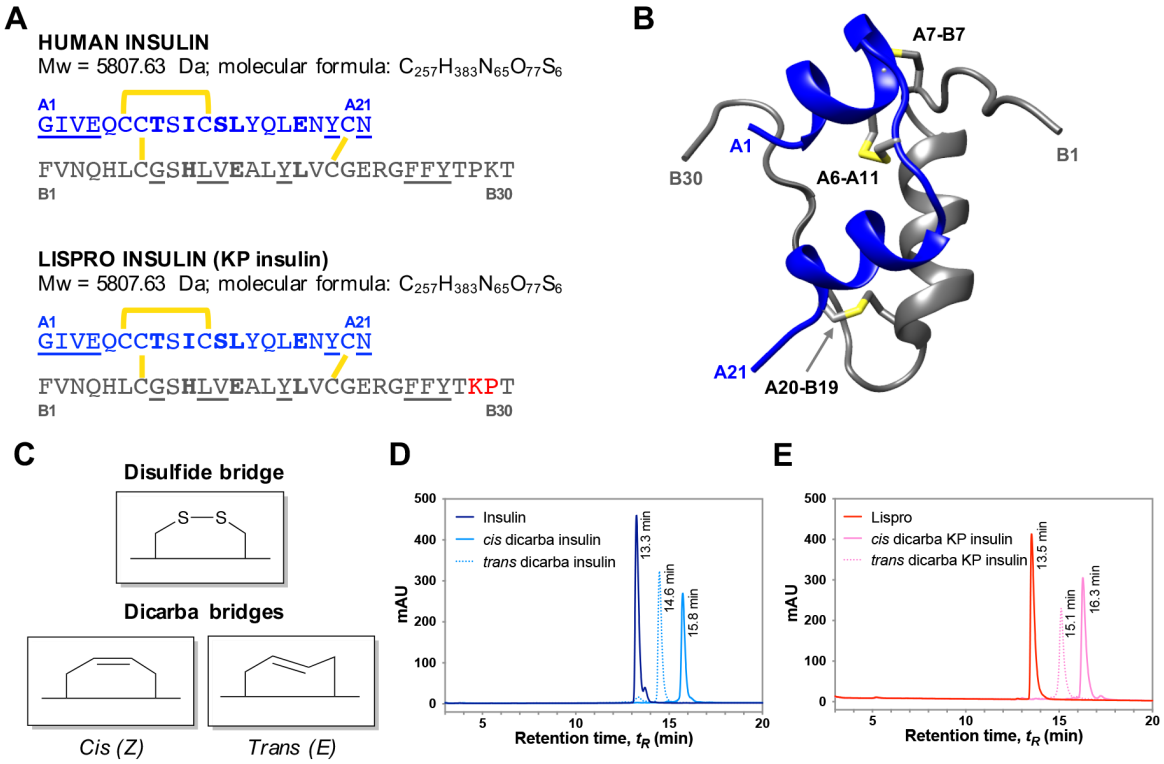

Figure 1. Insulin, KP insulin and dicarba insulin analogues. (A) Primary sequence comparison of human insulin (*top*) and KP insulin (*bottom*). Both consist of A (*blue*) and B (*grey*) chains stabilized by three disulfide bridges (yellow). *Underlined* are site 1-binding residues and *bold* are site 2-binding residues (17). Rapid-acting KP insulin has a reversal of B28 and B29 amino acids ($Lys^{B28}Pro^{B29}$) (*red*) compared to insulin. (B) Ribbon diagram of human insulin (2-Zn-coordinated T_6 conformation (20) PDB entry 1MSO) showing the location of the three α-helices (A chain: *blue;* B chain: *grey*) and the three disulfide bonds (*yellow*). (C) Schematic diagram of native cystine and isomeric *cis*- and *trans*-dicarba bridges. RP-HPLC chromatograms of (D) native insulin, *cis*- and *trans* dicarba insulins; (E) KP insulin, *cis*- and *trans* dicarba KP insulins.

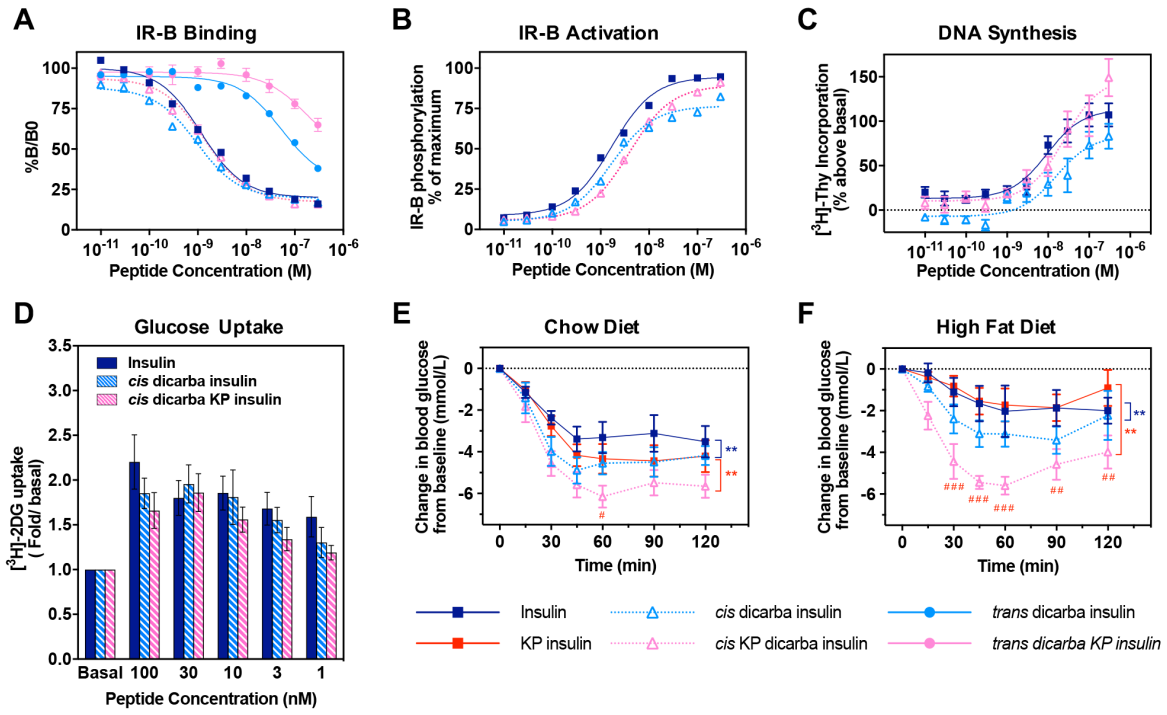

Figure 2. *In vitro* (A – D) and *in vivo* (E – F) activity of insulin, KP insulin and their respective dicarba insulin analogues. (A) Competition binding of insulin and dicarba insulins with europium-labelled insulin. Results are expressed as a percentage of binding in the absence of competing ligand (% B/B_0). (B) Activation of IR-B by increasing concentration of dicarba insulins (10 min stimulation) is expressed as receptor phosphorylation as a percentage of the maximal phosphorylation induced by insulin. Insulin *vs cis* dicarba insulin (ns); insulin *vs trans* dicarba insulin **** ($P \leq 0.0001$) (2-way ANOVA; Dunnett's multiple comparison) (C) DNA synthesis in response to increasing concentrations of dicarba insulins is shown as percentage incorporation of ^{3}H-thymidine (^{3}H-Thy) above basal. All data in (A –D) are the mean ± *S.E.M.* n = at least 3 independent experiments. (D) Glucose uptake stimulated by increasing concentrations of insulin, *cis* dicarba insulin or *cis* dicarba KP insulin is expressed as fold glucose uptake (pmol/min/mg) above basal. Insulin *vs cis* dicarba insulin *vs cis* dicarba KP insulin (ns) (paired *t*-test). (E) Insulin tolerance test in mice fed on a normal diet (chow), or on a high fat diet (HFD) were administered through intraperitoneal injection (*ip*) with 0.75 IU/kg insulin, KP insulin, *cis* dicarba insulin or *cis* dicarba KP insulin under non-fasting conditions and tail vein blood glucose was measured *via* glucose meter at indicated times. n = 5 – 6 per group. Blood glucose levels are expressed as change over basal levels (mmol/L). Chow diet: insulin *vs cis* dicarba insulin ** ($P \leq 0.01$); KP insulin *vs cis* dicarba KP insulin ** ($P \leq 0.01$) (paired *t*-test). High fat diet: insulin *vs cis* dicarba insulin ** ($P \leq 0.01$); KP insulin *vs cis* dicarba KP insulin ** ($P \leq 0.01$) (paired *t*-test). Significance of the change in blood glucose levels at each time-point was also determined by two-way ANOVA followed by Holm-Sidak's multiple comparison test. Chow diet: KP insulin *vs cis* dicarba KP insulin at $t = 60$ min $^{\#}$ ($p \leq 0.05$). High fat diet: KP insulin *vs cis* dicarba KP insulin at $t = 30$, 45 and 60 min $^{\#\#\#}$ ($p \leq 0.001$); $t = 90$ and 120 min $^{\#\#}$ ($p \leq 0.01$).

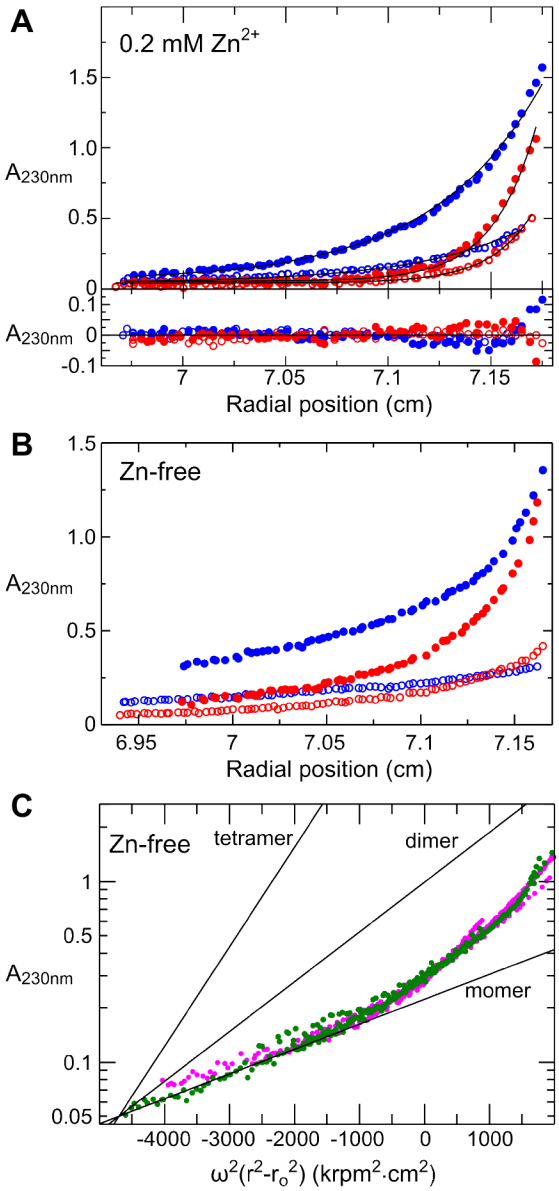

Figure 3. Sedimentation equilibrium data for *cis* dicarba insulin in the presence and absence of zinc ion (Zn^{2+}). Radial concentration distributions at sedimentation equilibrium for *cis* dicarba insulin in the (A) presence and (B) absence of 0.2 mM Zn^{2+} at loading concentrations of 100 (*open symbols*) and 300 µg/ml (*closed symbols*) at 25,000 (*blue*) and 40,000 rpm (*red*). In (A), data were globally fitted to a single species of 34,500 ± 400 Da (*solid lines*). Residuals to the fit (*bottom*) show some systematic deviation from an ideal fit. (C) Sedimentation equilibrium data for Zn-free *cis* dicarba (*green*) and native (*magenta*) insulin at each speed and loading concentration is plotted together as the square of the radial position scaled by rotor speed *vs* concentration on a logarithmic scale. The slopes expected for monomeric, dimeric and tetrameric insulin are shown for reference.

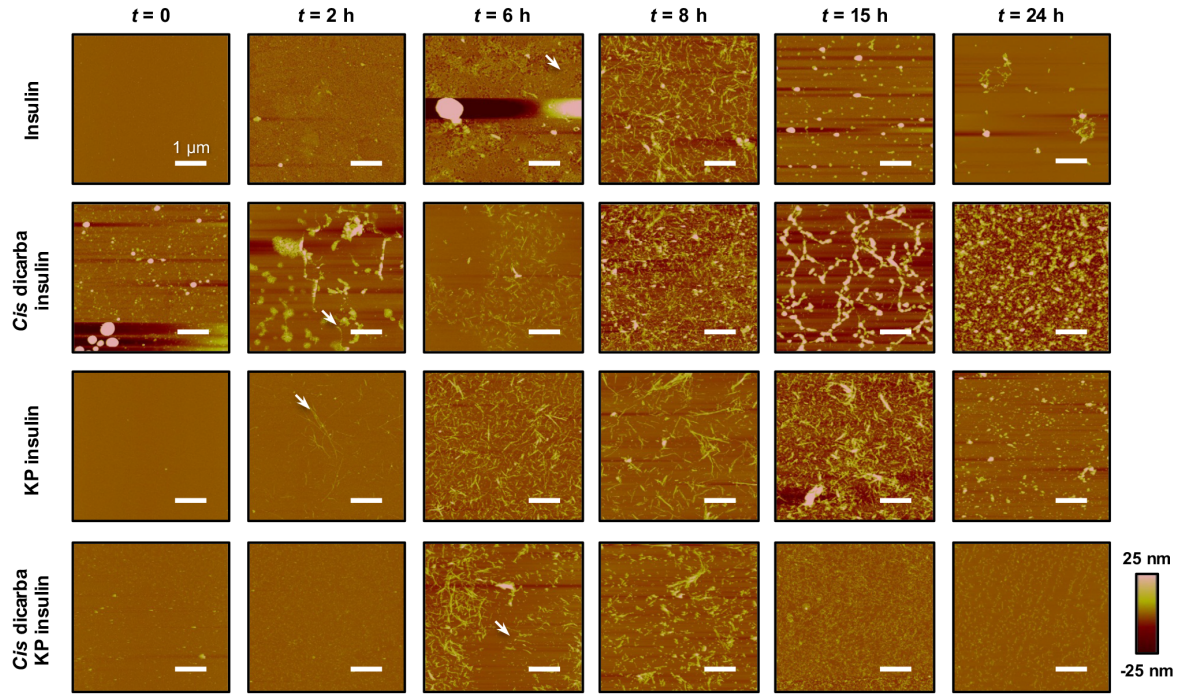

Figure 4. Time-course of fibril formation detected by AFM. Insulin fibrillation is first evident at t = 6 h. After t = 15 h, insulin has formed aggregates and fibrils are no longer easily detectable. Fibrillation of *cis* dicarba insulin is first evident after t = 2 h and is clearly detectable by t = 6 h. Fibrils formed by the *cis* dicarba insulin are of a different structure compared to insulin, particularly evident at t = 15 h. Fibrillation of the monomeric KP insulin is evident at earlier time-points across a wider incubation range (t = 2 – 15 h) compared to insulin. At t = 24 h, KP insulin fibrils are no longer easily detectable. Surprisingly, *cis* dicarba KP insulin fibrillation is only evident at t = 6 – 8 h with a rapid increase in formation of shorter and thicker fibrils at t = 6 h. In summary, the *cis* dicarba insulin adopts a different fibrillary pattern compared to insulin with an apparent increased complexity of fibrillary topology. These experiments are representative of n = 4 experiments for insulin, n = 3 for *cis* dicarba insulin, n = 5 for KP insulin and n = 3 for *cis* dicarba KP insulin. First detection of fibrils for each analogue is indicated by white arrows. The scale bar (*white*) corresponds to 1µm in all images.

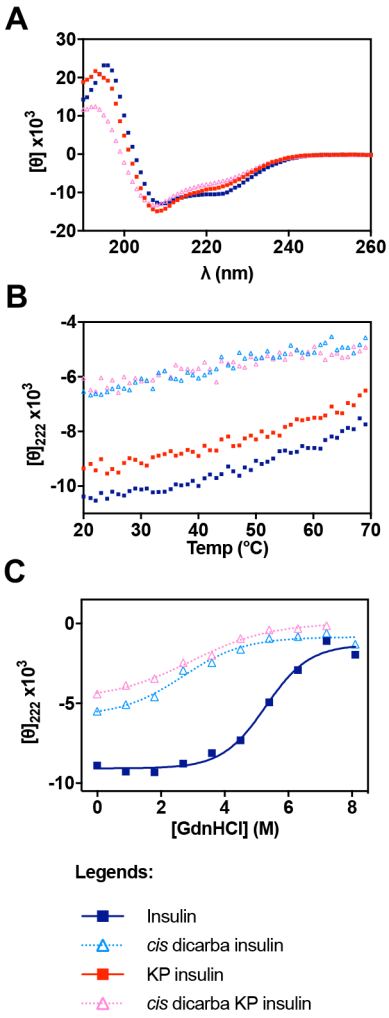

Figure 5. Thermal and chemical stability of *cis* dicarba insulin and *cis* dicarba KP insulin. (A) Circular dichroism far-UV spectrum of *cis* dicarba KP insulin suggests there is a difference in structure of the *cis* dicarba KP insulin compared to KP insulin and insulin, where lower helical propensities in the *cis* dicarba KP insulin is observed (see Table 1). θ = ellipticity. (B) Differences in thermal unfolding were monitored by ellipticity at λ = 222 nm and show both the *cis*- and *trans* dicarba insulins are considerably less stable than insulin. (C) Unfolding in the presence of guanidine hydrochloride demonstrates that both *cis* dicarba analogues are considerably destabilized compared to insulin. ΔG values derived from guanidine denaturation studies are listed in Table 1.

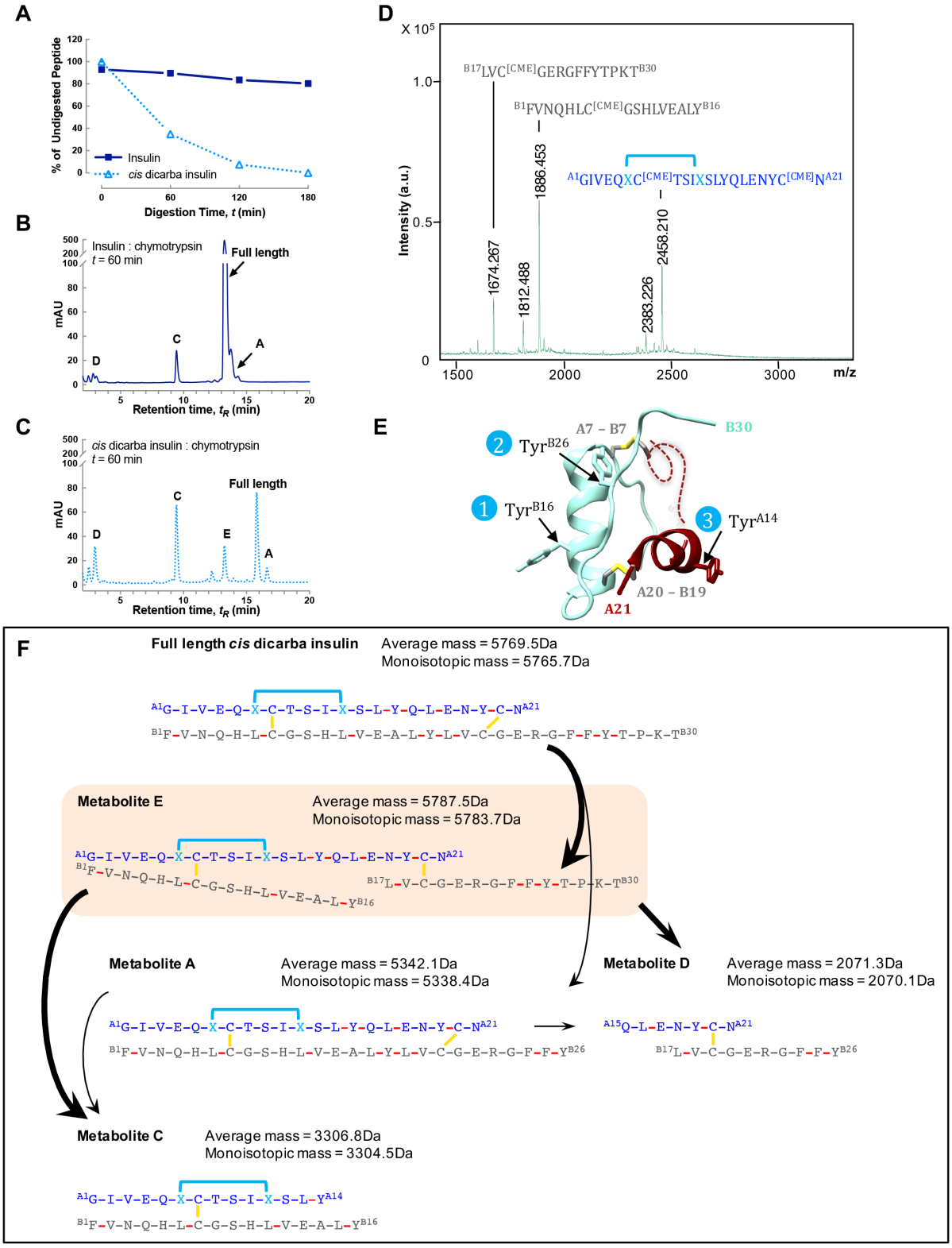

Figure 6. Limited proteolysis of insulin and *cis* dicarba insulin using chymotrypsin. (A) Rate of proteolysis plotted as percentage of undigested peptide over time. *Non-reducing* (B) insulin and (C) *cis* dicarba insulin digested for t = 60 min were analysed and fractionated using RP-HPLC. Metabolite **A** – **E** were identified *via* MALDI analyses in combinations of different conditions: whole sample *vs* RP-HPLC-fractionated samples; non-reducing *vs* reducing; positive *vs* negative detection mode (see Figs. S5 and S6). Indicated in (B), (C) and (F) are: full length, undigested peptide; metabolite **A**, non-reduced metabolite resulting from single cleavage at Tyr^{B26}; metabolite **C**, *C*-terminal- and metabolite **D**, *N*-terminal non-reduced metabolites resulting from cleavage at Tyr^{B26} followed by cleavages at Tyr^{A14} and Tyr^{B16}; metabolite **E** is only present in *cis* dicarba insulin cleavage reactions

and resulted from single cleavage at Tyr^{B16}. (D) Metabolite **E** of *cis* dicarba insulin was identified in fractioned sample proteolysed with chymotrypsin for t = 60 min. The sample was treated with DTT (reduction) and IAA (alkylation) prior to MALDI analysis under negative mode detection. [CME], Carboxymethylcystine residues with monoisotopic mass of 58.005 Da. (E) *Cis* dicarba insulin crystal structure (reported in (24); model coordinates not in the PDB database) with circled numbers indicating the order in which *cis* dicarba insulin peptide bonds are cleaved by chymotrypsin. (F) A simplified chymotryptic digestion kinetics of *cis* dicarba insulin showing sequences of peptides arising from chymotrypsin cleavage. A6-A11 dicarba bond (*blue solid line*). Insulin is cleaved first to metabolite **A** and then into metabolites **C** and **D**, with *no* metabolite **E** being detected. The rate of synthesis of each metabolite is presented in Figure S3 and S4. Subspecies of each metabolite were also identified *via* MALDI analyses (see Figs. S5 - 7).

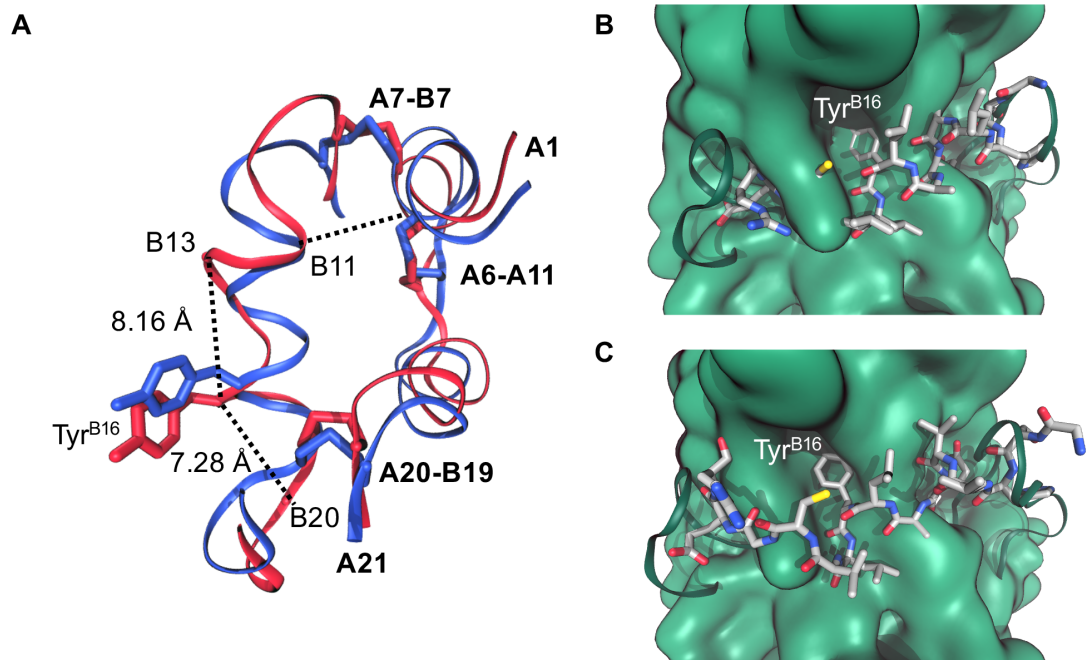

Figure 7. Bending of the B chain helix required to enable chymotrypsin proteolysis. (A) Overlay of the bent structure (*red;* MD simulation frame for *cis* dicarba insulin) with a reference insulin crystal structure (*blue*; PDB: 1MSO chains C and D). Residues A1 to A21 and B9 to B23 are superimposed. Hydrogen bonds in the B chain helix connecting residues Val^{B12} and Tyr^{B16}, Glu^{B13} and Leu^{B17} and Tyr^{B16}, and Gly^{B20} are broken, allowing the Cα-Cα distances between Glu^{B13} and Tyr^{B16} and between Tyr^{B16} and Gly^{B20} to increase from ~ 5.5 Å to > 7 Å. The bending rotates and compresses the A7-B7 disulfide bond and increases the distance between the *N*-terminal A chain and B chain helices (as measured by the Cα-Cα distance between residues A6 and B11). (B) Superimposition of the B chain helix of the un-bent insulin crystal structure (stick model; PDB: 1MSO chains C and D) on the active site of chymotrypsin (dark green; PDB: 4h4f – chymotrypsin in complex with inhibitor eglin C). For proteolysis to occur, Tyr^{B16} must be recognized by the active site of the enzyme. Superimposition of the backbone atoms of Tyr^{B16} as well as N and CA of Leu^{B17} on those of the corresponding residues in the inhibitor reveals that the un-bent structure cannot engage correctly with the peptidase: residues B12, B13 and all residues beyond B18 overlap significantly with the chymotrypsin structure, and the sidechain of Tyr^{B16} cannot sit properly in the active site cavity. (B) Superimposition of the B chain helix of the bent *cis* dicarba insulin simulation frame on the active site of chymotrypsin. Bulging of the B chain helix allows both the B12-B16 and B16-B20 loops to fit over the surface of the chymotrypsin molecule, with Tyr^{B16} sitting in the middle of the binding pocket. (Note: in both B and C the sidechains of B16, B17 and chymotrypsin residues 143 and 192 have been rotated to give the best possible engagement of the two molecules.) Loops of chymotrypsin which must move out of the way to allow insulin engagement are shown as *dark green ribbons*.

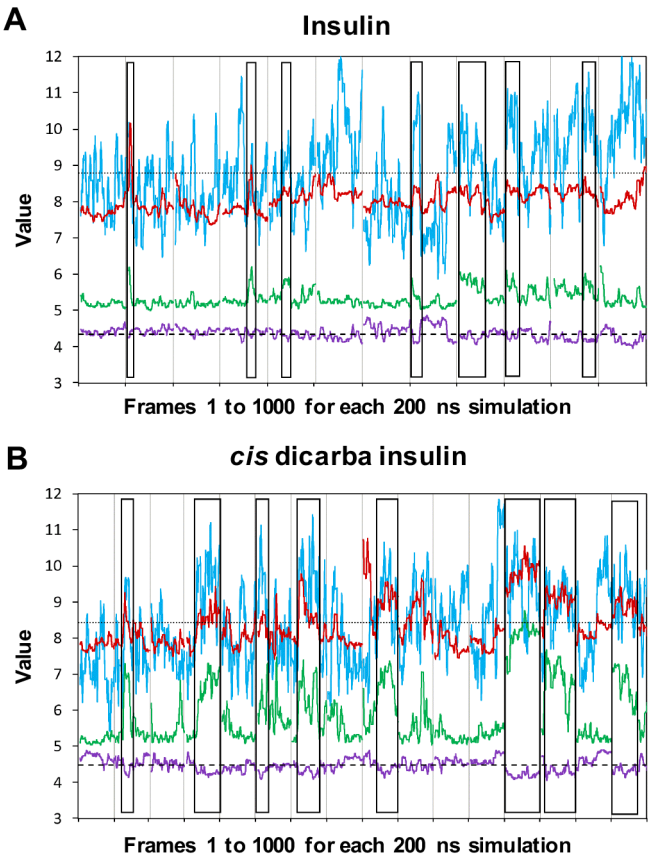

Figure 8. Variations in structural parameters associated with B chain helix bending from MD simulations. *Green*: *r*(Cα-Cα) between Glu^{B13} and Tyr^{B16}; this is a direct measure of helix bending. *Red*: *r*(Cα-Cα) between residue A6 and B11; a measure of the distance between the *N*-terminal A chain and B chain helices. *Purple*: *r*(Cα-Cα) between Cys^{A7} and Cys^{B7}; the length of the A7-B7 interchain linker. *Blue*: the relative torsional energy of the A7-B7 disulfide linkage. Data are presented as 50 period moving averages to highlight trends. Full data are presented in Figure S8. Overall averages for the purple and blue traces are shown with dashed and dotted lines, respectively. Bond distances are given in Å and relative torsional energies in kJ mol^{-1}. Bending events in the B chain helix are outlined in black boxes. Note that each bin on the horizontal axis represents an independent 200 ns simulations; traces are therefore not continuous between bins.

Probing the correlation between insulin activity and structural stability through introduction of the rigid A6–A11 bond

Shee Chee Ong, Alessia Belgi, Bianca van Lierop, Carlie Delaine, Sofianos Andrikopoulos, Christopher A. MacRaild, Raymond S. Norton, Naomi L. Haworth, Andrea J. Robinson and Briony E. Forbes

J. Biol. Chem. published online June 13, 2018

Access the most updated version of this article at doi: 10.1074/jbc.RA118.002486